Study of the Exotic Ground State Physics in XXZ Quantum Spin Ice

by

Alexandre Gérard Raymond Day

A thesis
presented to the University of Waterloo
in fulfillment of the
thesis requirement for the degree of
Master of Science
in
Physics

Waterloo, Ontario, Canada, 2014

© Alexandre Gérard Raymond Day 2014

I hereby declare that I am the sole author of this thesis. This is a true copy of the thesis, including any required final revisions, as accepted by my examiners.

I understand that my thesis may be made electronically available to the public.

Abstract

Three dimensional frustrated magnets realized in the rare-earth pyrochlores ($R_2B_2O_7$, R =rare-earth ion, B = transition metal ion) have attracted much interest since the discovery of spin ice in $Ho_2Ti_2O_7$ [1]. Since then, a number of interesting phenomena in pyrochlore magnets have been observed and the interest in these systems, from an experimental and theoretical point of view, has nothing but increased. Perhaps the most appealing and unique possibility is that these systems may realize a quantum disordered phase; a so-called quantum spin ice. Theoretically, it has been predicted that a $U(1)$ quantum spin liquid is realized in the XXZ quantum spin ice (with global $U(1) \times \mathbb{Z}_2$ symmetry) in the perturbative regime [2] and more recently Savary and Balents [3] have introduced a quantum rotor model with bosonic spinons coupled to $U(1)$ gauge fields to describe non-peturbatively the deconfined phase predicted. They studied an anisotropic quantum spin ice (QSI) model which corresponds to the XXZ QSI with an additional $S_i^z S_j^x$ coupling. They solved the quantum rotor model using a mean-field approximation combined with a large-N approximation and predicted the possibility of a $U(1)$ liquid in addition to an exotic ferromagnetic phase. Further work [4] has addressed the more complicated fully frustrated XXZ quantum spin ice regime, where all components of the model are frustrated, by using some insights provided by the previous perturbative results.

In this thesis, we will address the non-perturbative regime of the fully frustrated XXZ QSI beyond the simplest perturbative treatment. We will begin by mapping the quantum spin ice model to a compact $U(1)$ gauge theory with deconfined electric and magnetic monopoles. Neglecting the interaction between the gapless photon excitation and the electric charges, we will study the matter sector with only electric charges, the so-called spinons. Building up on insights provided by high order degenerate perturbation theory calculations, we will construct some symmetric spin liquid *ansatz* for the static part of the gauge fields. The two novel spin liquids that we construct break time reversal symmetry and thus have a non-trivial chirality. In order to solve the matter sector of the theory and determine the stability of the deconfined phases, we will introduce a novel representation of a XY quantum rotor in terms of "exclusive" bosons, a representation which is dynamically implemented in the dilute limit. We will benchmark this mapping in different ways by comparing our results with Quantum Monte Carlo simulations and exact diagonalization in some limiting cases. Using this mapping we will compute the region of stability of the $U(1)$ liquid phase of XXZ QSI. Within this mapping we will reproduce qualitatively the results of previous work by finding only the so-called zero and π flux $U(1)$ liquids in the vicinity of the classical spin ice point, while improving greatly on the estimation of the exchange coupling at which the bosonic spinons condense to form a superfluid phase. In

the fully frustrated XXZ QSI, we will provide evidence, using exact diagonalization of the quantum rotor model, that one of the chiral spin liquid may be realized in the strongly correlated and frustrated QSI regime, where all previous approximations break down.

Acknowledgements

To some extent, physics at the level of graduate studies is about developing relationships, learning and exchanging ideas with various graduate students, lecturers and professors. All in all, the path on which I acquired new knowledge and that has led to the writing of this work has been paved by many different individuals that I am very honoured to have met and that I am looking forward to continue exchanging ideas and sharing experiences with.

First and foremost, I am delighted to acknowledge the person who supervised my endeavours, Professor Michel Gingras. He gave me almost absolute freedom to explore many different projects and has taught me, over many long, sometimes tedious discussions, many virtues of what it is to be a scientist. I think it is fair to say that Professor Gingras is a very passionate physicist.

Another great contributor to my work is Dr. Zhihao Hao who I started working with extensively only half a year prior to the writing of this thesis but who has helped enormously in my understanding of gauge theories and quantum spin-ice. I cannot refrain to mention my friend and colleague Dr. Behnam Javanparast, with whom I had a delightful experience calculating sixth order high-temperature expansions, writing papers and discussing various aspects of science, life and work. I would also like to acknowledge Dr. Taoran Lin, whose been a great reference for any question about dipolar spin-ice and statistical physics.

Although I was working in Waterloo, I have kept a great bond with the people at the Université of Sherbrooke. I am pleased to thank both prof. David Sénéchal and prof. André-Marie Tremblay, from who I have learned so much in my many exchanges with them (over the course of my undergraduate and graduate studies) and that are in great part responsible for my interest in the field of computational physics and the theory of condensed matter. I also warmly acknowledge the great students in Sherbrooke, in particular my friends Maxime Dion and Maxime Charlebois.

I would also like to thank Professor Roger Melko and Lori Woolner. Prof. Melko has taught me two wonderful condensed matter courses but also that it is possible to combine physics and fun. Lori has always been very kind to me and has contributed in making my Waterloo experience memorable.

My family has been very supportive in this work. My mom has always made sure that my "projects" were going well and has been extremely kind in helping me in planning my future graduate studies. My dad, as a man of science himself, has been influential in my way to perform my work. Over the years, I have benefited from his advice and he significantly contributed in given me the confidence to pursue a career, as far as I can, in academia. My younger sister, in her passion for discovering the world but also in many

different aspects, has also greatly inspired me. My older sister has also been supportive in my endeavours and I am much looking forward to visit her again in Lanzarote.

Finally, I would most particularly like to thank my girlfriend Ann-Marie. Her love, her support and her diligence in her own studies have been vital elements behind my motivation for often working long hours.

I am also much grateful to my friends and colleagues in Waterloo and back home for their constant support: Guillaume, Rémy, Justin, Félix, Othman, David, Bohdan, Lauren, Andrew, Halle, Grant, Mohan, Ann, Kay and Katja.

To my family and my friends

Table of Contents

List of Tables

List of Figures

The content of the following chapter of this thesis is the outcome of a collaboration with Dr. Zhihao Hao. The author of this thesis is responsible for the perturbation theory calculations, the large-N study of the XXZ quantum spin ice in search for chiral spin liquids and exact diagonalization results. The author has also contributed in the investigation for determining the flux *ansatz* and methods to improve the approximation schemes in solving the quantum rotor model. The author was also involved in the study of the interaction term between gauge fields and spinons. The author of this thesis also coauthored the following work published during the completion of his degree:

1. Resilience of d-wave superconductivity to nearest-neighbor repulsion, Phys. Rev. B **87**, 075123 (2013) where I performed cluster dynamical mean-field theory calculations to obtain and demonstrate the main result of the paper : d-wave superconductivity is resilient to neareast-neighbour repulsive interactions in the $2D$ Hubbard model. This work was also presented by the author at the 2014 March Meeting in Denver.

2. Phase transition and thermal order-by-disorder in the pyrochlore antiferromagnet $Er_2Ti_2O_7$: A high-temperature series expansion study, Phys. Rev. B **88**, 220404 (2013) where I performed the degenerate perturbation theory calculations to obtain Van-Vleck susceptibility corrections to the high-temperature expansion obtained by the main authors. Combining our results, we obtained a good agreement with experimental data, thus confirming (a) that $Er_2Ti_2O_7$ is well described by the effective $S = 1/2$ Hamiltonian presented in (1.21) and (b) that $Er_2Ti_2O_7$ orders via a thermal order-by-disorder mechanism.

3. Thermal Order-by-Disorder at Criticality in XY Pyrochlore Magnets, to be submitted to Phys. Rev. B. Introducing a somewhat novel exact diagonalization method combined with a mean-field boundary condition, I obtained a phase diagram that describes qualitatively the effect of order-by-disorder in the anisotropic spin-1/2 pyrochlore lattice Hamiltonian. My results complemented the work of the first author and guided part of his, in particular in determining some subtle symmetry allowed terms that arise in the Ginzburg-Landau treatment. I also contributed to the calculations of the main author in deriving a method to compute high-temperature expansion diagrams using tools from graph theory.

The contributions of the author in these works are not presented in this thesis due their different subject matter from the main theme of this thesis.

Chapter 1

Introduction

1.1 Frustrated magnets

The past decades have seen a flurry of interest for systems of condensed matter whose effective low-energy degrees of freedom are spins that interact in such a way that all classical pairwise interactions of the Hamiltonian of the system cannot be simultaneously satisfied: these systems are referred to as *frustrated* magnets [5]. In the particular case where the geometry of the lattice (see Fig. 1.1) at the vertices of which the spins reside is responsible for frustrating the interactions, the system is said to be *geometrically* frustrated [6, 7, 8]. Perhaps the characteristic property of frustrated magnets is that they posses a ground state with a large, often extensive degeneracy which in turns leads to a *residual* entropy. This residual entropy may often be estimated by considering only the *classical* ground state of the simplest frustrated units that span the lattice of the frustrated system. This means that the low-energy physics of these systems is analogous to that of a liquid or a *cooperative paramagnet* [9]: while the system remains disordered, the spins at small distances are strongly correlated so that their fluctuations are largely constrained. These correlated states generally share a "pattern rule" which constitute the corner-stone of the interesting physics arising in frustrated systems. One of the characteristic experimental signatures of frustration is the ratio of the Curie-Weiss temperature (θ_{CW})[1] to that of the ordering temperature of the system T_c – if ordering is indeed observed. When $T_c \ll \theta_{CW}$, the system is typically said to be highly frustrated [10].

[1] Which is a measure of the strength of the spin-spin interactions.

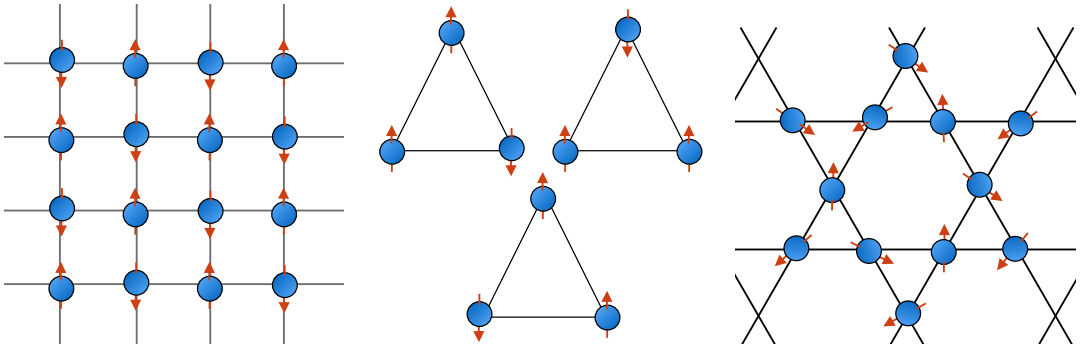

(a) (b) (c)

Figure 1.1: Examples of how geometry can lead to frustration in systems with nearest-neighbour antiferromagnetic interaction. (a) A bipartite lattice is a non-frustrated lattice. We can choose one sublattice to be pointing up and the other to be pointing down to satisfy all interactions. (b) A triangle is an example of frustrated geometry. It is impossible to simultaneously anti-align all spin on the triangular which leads to a 6 fold degeneracy of the ground state of the triangle. (c) The kagome lattice (non-bipartite) is formed of triangular motifs that lead to frustration.

1.2 Spin ice

One of the landmarks of frustrated magnetism is *spin ice* [5]. Spin ice was discovered in $Ho_2Ti_2O_7$ [1] and bears it's name from a direct correspondence to one of the disordered phases of crystalline water-ice in which the oxygens adopt a tetrahedrally coordinated geometry and remain disordered down to very low temperatures. The system exhibits a residual entropy which originates from the frustration of the protons of the hydrogen atoms that are shared between each pair of oxygen O^{2-} ions. In the tetrahedral geometry, each oxygen must have *only* two protons in it's vicinity: this is one of the famous Bernal-Fowler ice-rule [11]. In spin ice the role of the protons is played by the magnetic moment of the rare-earth Ho^{3+} or Dy^{3+} ions that form a pyrochlore lattice (see Fig. 1.2). The Ti^{4+} ions are non-magnetic and reside on another pyrochlore lattice that is interpenetrating with the former rare-earth ion pyrochlore lattice. The oxygens that surround the Ho^{3+} or Dy^{3+} are responsible for generating a strong crystal field single-ion anisotropy along the local $\langle 111 \rangle$ directions of each tetrahedron vertices (see Appendix A for specific details about the geometry). As a result, the large and classical f-electron spin moment of the rare-earth ions is forced to point either towards the center of it's corresponding tetrahedron or opposite to that direction. Although the relevant interactions in $Ho_2Ti_2O_7$ and $Dy_2Ti_2O_7$

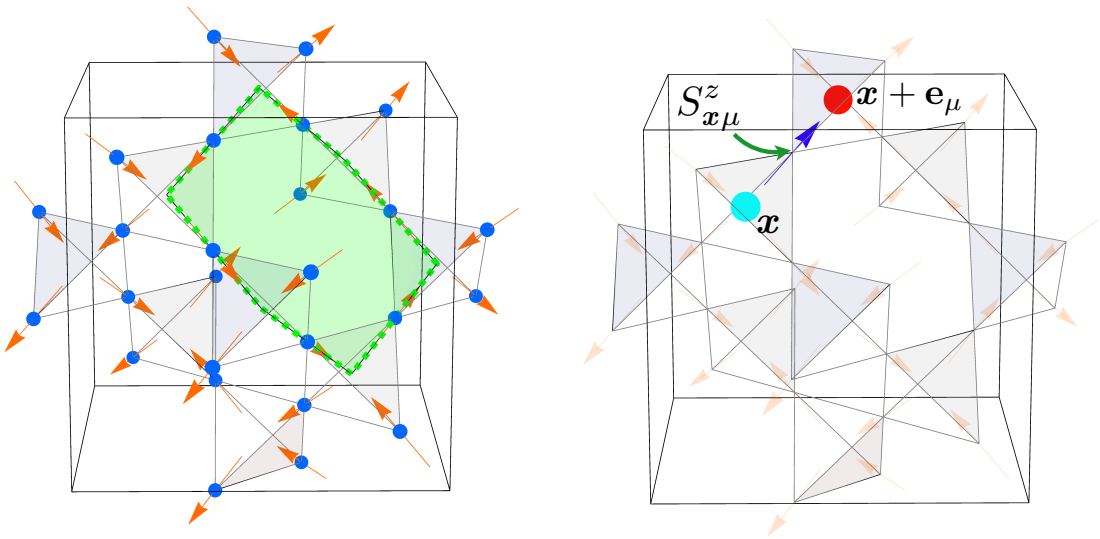

(a) (b)

Figure 1.2: (a) The pyrochlore lattice with spins in a spin ice (2-in/2-out) configuration. Following the spins head to tail we can form closed loops, the smallest of which form hexagonal plaquettes (emphasized in green). When flipping all spins that constitute that loop, we go from one spin ice state to another spin ice state. (b) Considering the spin ice states as some correlated vacuum background, the elementary excitations of such a vacuum come in pairs of a positively (say the red sphere) and negatively (say the cyan sphere) charged defects that are generated by a single spin-flip. These defects live on the diamond lattice which is formed by connecting the center of the tetrahedra of the pyrochlore lattice.

are dipolar in nature, much of the physics of spin ice can be discussed within the context of a nearest-neighbor ferromagnetic Ising model with a local [111] anisotropy ($\vec{S}_i = S_i^z \hat{e}_i$) [12, 13]:

$$H_{\text{spin ice}} = J_{\text{nn}} \sum_{\langle ij \rangle} \vec{S}_i \cdot \vec{S}_j = -\frac{J_{\text{nn}}}{3} \sum_{\langle ij \rangle} S_i^z S_j^z \qquad (J_{\text{nn}} < 0). \tag{1.1}$$

The unit vectors $\{\hat{e}_i\}$ point along the $\langle 111 \rangle$ directions (see Appendix A) and S_i^z corresponds to the *local z-component* of the spin $\vec{S}_i$. The ferromagnetic spin-spin interaction J_{nn} is frustrated owing to the Ising anisotropy axes[2]. This in turn leads, as in real water-ice, to

[2]Hereafter we will use $J_{zz} = -J_{\text{nn}}/3$, with $J_{\text{nn}} > 0$ to denote the spin ice interaction.

a residual entropy at low temperatures, thus breaking the third law of thermodynamics. Spin ice is commonly referred to as a classically disordered cooperative paramagnet [13].

This residual entropy may be estimated via a single-tetrahedron picture as it was first done in a seminal paper by Linus Pauling [14]. One isolated tetrahedron has 16 possible configurations (see Fig. 1.3) and the spin ice Hamiltonian favors a six-fold degenerated ground state with 2 spins pointing inwards and 2 spins pointing outwards (2-in/2-out). The first excited state corresponds to a 3-in/1-out or 3-out/1-in configuration. Considering a system of N spins, there are $N/2$ tetrahedron that span the pyrochlore lattice (since each spin is shared between two inversion-related tetrahedra). Neglecting the correlations in between each tetrahedron, it is possible to find an upper-bound for the extensive ground state entropy[3] of spin ice:

$$S(T=0) = \ln\left[\left(2^N\right)\left(\frac{6}{16}\right)^{N/2}\right] \approx \frac{N}{2}\ln\left(\frac{3}{2}\right). \tag{1.2}$$

This is the so-called Pauling residual entropy. In an experimental setting, the residual entropy (per mol) is determined by integrating the specific heat, $C(T)$:

$$S(T^*) = R\ln 2 - \int_{T^*}^{\infty}\frac{C(T)}{T}\mathrm{d}t, \tag{1.3}$$

where $S(T=\infty) = R\ln 2$ (for a $|\vec{S}| = 1/2$ spin system), $R = 8.31$ J·mol^{-1}K^{-1} in SI units and where T^* is the lowest temperature reached in a particular experiment measuring the specific heat.

The Pauling entropy of Eq. (1.2) has been measured within in a few percent accuracy[4] to be the residual entropy of the $Ho_2Ti_2O_7$ and $Dy_2Ti_2O_7$ spin ice compounds [17, 18, 19].

[3]Note that in this thesis I adopt the following convention for the analytical results: $k_B = 1, \hbar = 1$. When discussing experimental results, I restore the physical units.

[4]Recent work by Pomaranski *et al.* has shown that these compounds may eventually order at very low-temperatures [15], which is partially in agreement with the expectations that these compounds are described by a dipolar spin ice model [16].

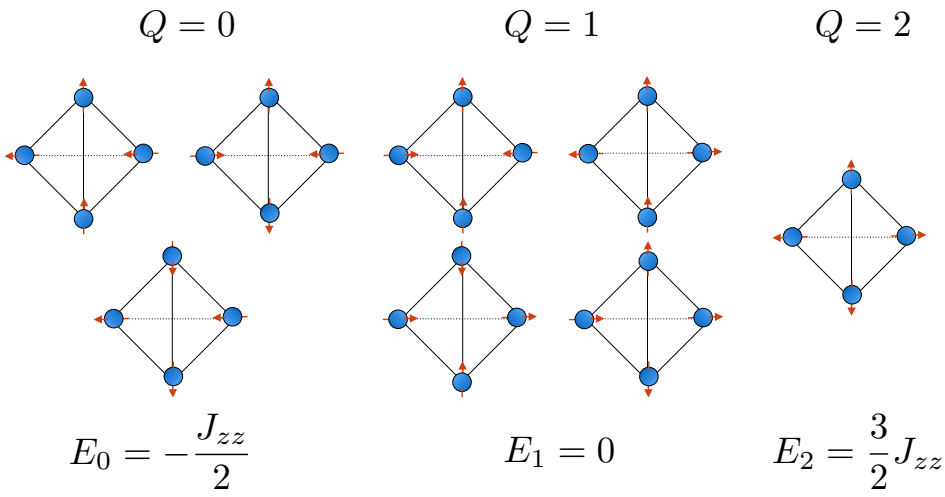

Figure 1.3: Eight of the sixteen configurations of the Ising spins of Hamiltonian (1.1) for a single tetrahedron (the time-reversal conjugate partners are omitted) with $S_i^z = \pm 1/2$. The ground state with energy $E_0 = -J_{zz}/2$ corresponds to the 2-in/2-out configuration while the first excited state is a 3-in/1-out or 3-out/1-in configuration with energy $E_1 = 0$. The configuration with highest energy is the all-in/all-out configuration with energy $E_2 = 3J_{zz}/2$. The charge Q assocatied with these states (see Eq. (1.19)) is also indicated.

1.2.1 Emergent electromagnetism in spin ice

We can gain further insights by thinking of the spin ice rules, which enforce a 2-in/2-out spin configuration per tetrahedra, as lattice *divergence-free* condition [12]. Indeed, interpreting the spins as electric field variables[5] , i.e. $E^z \equiv S^z$, then we may write:

$$\sum_{\mu=0}^{3} S^z_{\boldsymbol{x}\mu} = 0 \Leftrightarrow \nabla \cdot \vec{E^z} = 0 \tag{1.4}$$

where we use $\boldsymbol{x}$ to denote the diamond lattice site (see Fig. 1.2) coordinates and $\mu = 0, 1, 2, 3$ to denote the pyrochlore sublattice basis (see Appendix A). The spins of the original pyrochlore live on the bonds of the dual diamond lattice and we use $\boldsymbol{x}, \boldsymbol{x} \pm \mathbf{e}_\mu$ to

[5]Note that in what follows, I will use the language of electric charge to describe the spin ice defects instead of "magnetic monopole", which is the term used in the spin ice community [20] . Because electric field and magnetic field are dual in electromagnetism, this will not influence any results. The magnetic monopole in our description is a somewhat more complicated type of excitation that I will describe in subsequent sections.

denote the spin that lives on the bond that joins the diamond site $\boldsymbol{x}$ and $\boldsymbol{x} \pm \mu$. Then, $S^z_{\boldsymbol{x}\mu}$ is a shorthand notation for $S^z_{\boldsymbol{x},\boldsymbol{x}+\eta_{\boldsymbol{x}}\mathbf{e}_\mu}$ with:

$$\eta_{\boldsymbol{x}} = \begin{cases} 1 & \text{if } \boldsymbol{x} \in \langle a \rangle \\ -1 & \text{if } \boldsymbol{x} \in \langle b \rangle \end{cases} \tag{1.5}$$

where $\langle a \rangle$ and $\langle b \rangle$ correspond to the two FCC lattices that form the diamond lattice.

The physics of spin ice corresponds to the physics of *closed loops* of electric field lines (see Fig. 1.2) and total electric field of the spin ice configurations labels different topological sector of the spin ice manifold. The fluctuations in the spin ice manifold are highly correlated and to fluctuate from one spin ice state to another, one needs to flip all spins around a closed loop simultaneously. The smallest loops that encodes such fluctuations are hexagons. These type of fluctuations will be discussed in greater details in the context of quantum spin ice.

A 3-in/1-out or 1-in/3-out configuration for a single tetrahedron is then naturally interpreted as the source of this electric-field, i.e. an *electric charge*. This electric charge lives on the diamond lattice (see Fig. 1.2) that is dual to the pyrochlore lattice. Electric charges can only be created in pair: a spin ice defect corresponds to the creation of a positive *and* negative electric charge. One the most remarkable feature of spin ice is that the spin-spin correlation function exhibits a power-law dipolar-like ($\propto 1/r^3$) correlation [12]. In reciprocal space, this translates into a static structure factor with "pinch points" at the reciprocal lattice vectors (see Fig. 1.4). These pinch points have been observed in neutron scattering experiments [21]. Finally, in the case of nearest-neighbor spin ice the, the electric charge defects do not interact with each other and are thus deconfined. Here by deconfined, we mean the following. Within the language of gauge theories, two test charges are said to be deconfined if the potential energy cost required for separating two charges over a macroscopic distance is finite [22]. In the case where the dipolar interactions are also taken into account, it has been shown that the general properties mentioned above are preserved, althought the interaction potential between the defects follows Coulomb-law [20] which leads to an effective non-confining "tension" between pairs of electric defects. All in all, it may be said that electromagnetism is an emergent property of spin ice, i.e. it corresponds to an effective low energy description of spin ice. This description will be pursued in subsequent sections, where we will see that quantum fluctuations in quantum spin ice leads to an emergent quantum electrodynamics (QED) type of theory [2, 3, 23, 24] in the form of an exotic quantum disordered phase: a $U(1)$ *quantum spin liquid*.

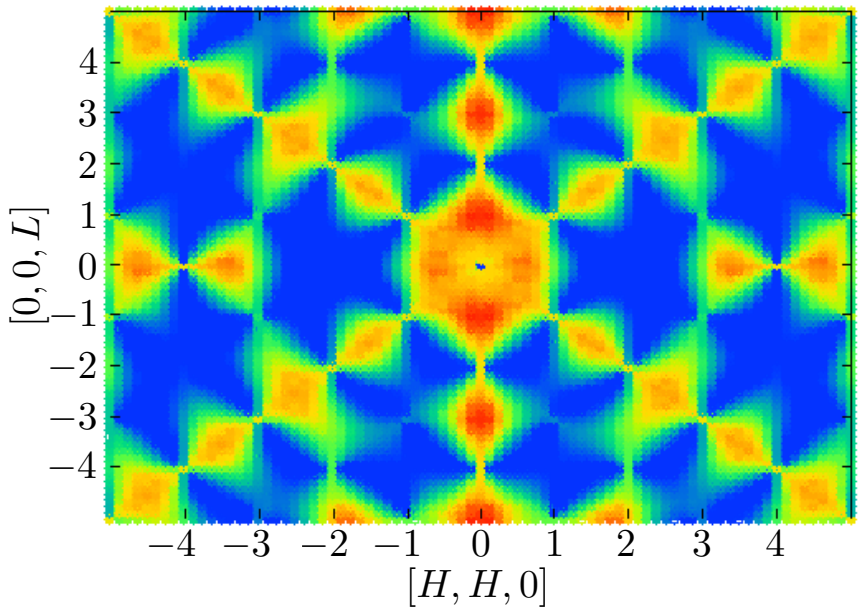

Figure 1.4: [This figure is a courtesy of Taoran Lin] Elastic neutron scattering structure factor computed for pure dipolar spin ice in the spin-flip channel [21]. The pinch points correspond to the singularities at the reciprocal lattice vectors $[h, h, l]$, with $n, h = \pm 1, \pm 2, \cdots$.

1.3 Quantum spin liquids

In the following sections we make a small digression to introduce the concept of quantum spin liquids from an historical perspective. We will then introduce the concept of projective construction for spin liquids and it's relation to gauge theories. We will then discuss these ideas in the context of quantum spin ice.

1.3.1 Frustration and quantum disorder

It has been known for some time [25] that a small value of spin length (S) combined with geometric frustration effectively enhance quantum fluctuations (see Fig. 1.5 and Fig. 1.6) [26]. Indeed, in 1972 Anderson studied the $S = 1/2$ Heisenberg antiferromagnet on the triangular lattice and provided evidence that a state with large quantum fluctuations and with *no broken-symmetries*, the so-called *resonating valence bond* (RVB), may be an

alternative ground state to a conventional (semi-classical) long-range Néel order [26]. The RVB state (see Fig. 1.7), which corresponds to a large superposition of different singlet lattice coverings, may be interpreted as a quantum liquid since it corresponds to a "melting" of some symmetry breaking state via quantum fluctuations. In particular, the RVB state corresponds to a "melting" of a *valence bond crystal* (VBC) [27].

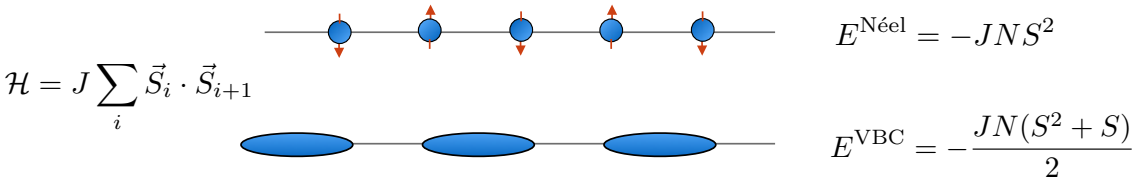

Figure 1.5: Example of the effect of spin length in inducing quantum fluctuations for the Heisenberg antiferromagnetic spin chain. A simple *variational* wave-function shows that for $S = 1/2$, a valence bond crystal formed of nearest-neighbour singlets is favored over a Néel state while for $S > 1$ the Néel state is favored over the VBC state. Althought in one dimensions one cannot have long-range order such as a Néel order [28], this simple example illustrates that system with small value of spin S may exhibit more "quantumness" than the system with large S limit. The VBC forms a natural building block for quantum non-magnetic state as it is formed of $S = 0$ singlets (see Fig. 1.7) [13].

The idea of RVB remained relatively undiscussed until 1987, when it was dramatically revived with the discovery of the *cuprates* and their high-temperature superconducting properties [29] realized when *doped*. The proximity of the cuprates to a metal-insulator transition (so-called Mott transition) hinted that the mechanism behind the unusual appearance of superconductivity[6] at high temperatures might be related to a RVB ground state, the excitations of which becomes charged superconducting pairs when the system is doped [31].

While the initial motivation to link quantum spin liquid with the appearance of high-temperature superconductivity has somewhat faded out in the recent years, the search for quantum spin liquids as a ground state of a quantum spin Hamiltonian has, conversely, gathered much interest over the years. This is in part due to the fact that these states are intrinsically correlated and have some form of entanglement, making them challenging to study. Along with these generic properties, quantum spin liquids are expected to exhibit some kind of topological order and generically host fractional excitations [32]. By fractional

[6]Meaning that such high T_c seemingly cannot originate from an electron-phonon coupling as in conventional superconductors [30].

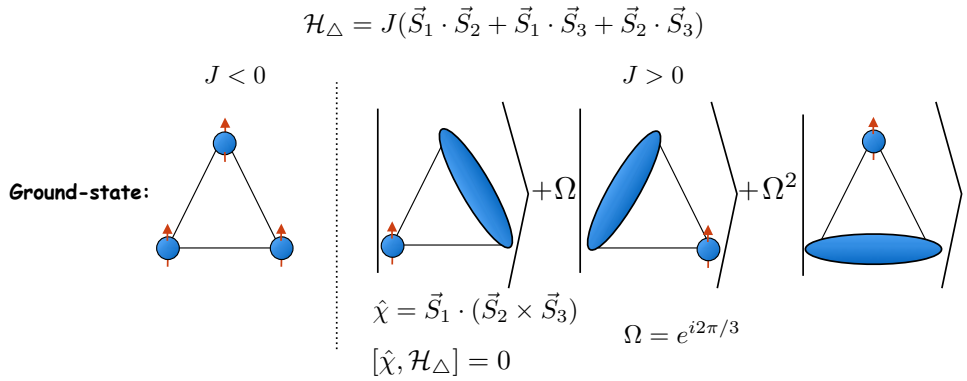

Figure 1.6: Heisenberg model for a triangle unit. In the ferromagnetic case, the interaction is not frustrated and the ground state corresponds to simply having all spin aligned along an arbitrary direction. In the antiferromagnetic case, the ground state is chiral ($\hat{\chi} = \pm 1$) and may be interpreted as having an unpaired fermion (spin 1/2) moving around the triangle.

here, we mean that these excitations carry quantum numbers that are a fraction of the allowed quantum number for a finite system [33]. The fact that these exotic[7] state may have potential applications in quantum computation further increase their interest [34, 35]. The essential idea in the field of topological quantum computation using (gapped) spin liquids is that these states possess a ground-state degeneracy that is protected by the topology of the system. This makes these states appealing for quantum computation due to their robustness against decoherence [34, 35].

1.3.2 The limitations of the Gingzburg-Landau paradigm

One of the simplest (and crudest) starting point to study condensed matter system is the so-called mean-field theory (MFT). MFT consist in replacing an original many-body problem with a simpler problem of a *self-consistent* one-body system interacting with an averaged field produced by the rest of the interacting degrees of freedom, neglecting the fluctuations of the averaged field [36].

MFT is equivalent to a Ginzburg-Landau theory (this equivalence may be shown via a Hubbard-Stratonovich transformation) and is based on the existence of a *local order parameter* that carries a non-trivial irreducible representation of the symmetry group of the

[7] Exotic in the sense that they support fractional excitations.

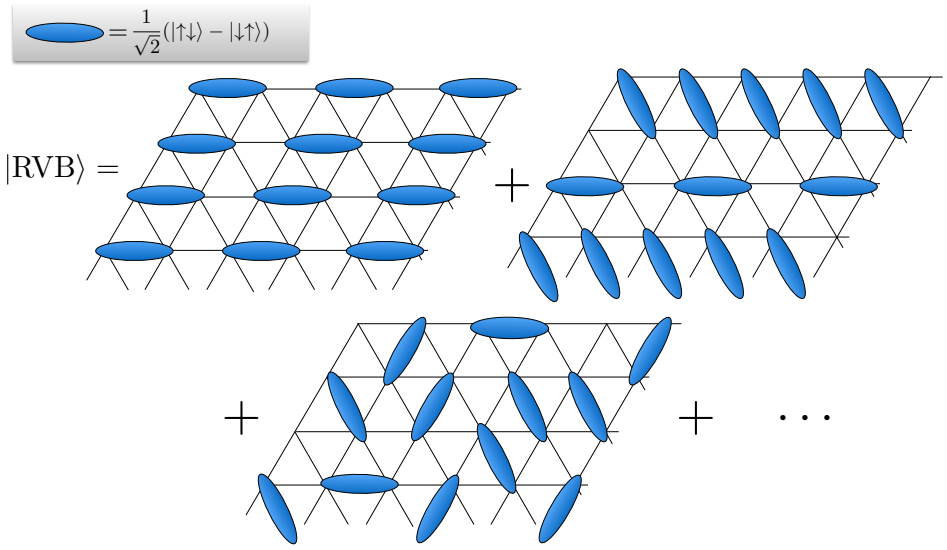

Figure 1.7: Example of a *short-range* resonating valence bond state on the triangular lattice. It consist of a superposition of all possible singlet covering and does not break $SU(2)$ symmetry or space group symmetries.

Hamiltonian. The order parameter is generally an expectation value of some combination of the degrees of freedom of the system. For example, a ferromagnet has a finite overall magnetization that breaks time-reversal symmetry. When the order parameter develops a finite expectation value, it indicates that the system is in a symmetry-broken state. The measurement of the different possible order parameters then allows one to construct a phase diagram which classifies the different state that the system enters depending on the values that the parameters of the system's Hamiltonian take .

However, since the discovery of the fractional quantum-Hall (FQH) effect [37], it has been known that not all phases of matter may be understood via the concept of symmetry breaking [38]. In fact, in the case of the FQH effect, the concept of topological order had to be introduced to understand what characterizes the FQH state [39] since this state does not break any symmetry. The concept of topological order applies to *gapped* phases[8] of matter at zero temperature [32]. While topological order describes a certain type of quantum order, the general theory of quantum order appears to be far richer [38, 32].

Quantum spin liquid states may be gapped or gapless and recent state of the art numerical studies have provided strong evidence for the existence of such state in $D > 1$

[8]Meaning that the thermodynamic system has ground state with a finite gap for any excitation [32].

for the $S = 1/2$ $J_1 - J_2$ kagome Heisenberg antiferromagnet [40]. Other examples of such state in more intricate but yet, *exactly solvable* quantum models, have been provided by A. Kitaev, M. Levin and X.G. Wen. [32, 34] The solution of Kitaev's model uses a trick that was first discussed by Baskaran *et al.* [27, 41] in order to extract the physical properties of the RVB state. This trick is formally known as the *projective construction* or *slave-particle* method.

1.4 MFT of quantum spin liquids and emergent gauge theory

As mentioned in the previous section, mean-field theory fails to describe any QSL state since such a state does not break any symmetry of the Hamiltonian. The latter somewhat negative definition of a QSL implies that the excitations of a QSL must carry some fractional quantum number [42, 32] (otherwise these excitations would be related to the fluctuation of some order parameter). Assuming the existence of QSL, it is then natural to try to understand it's properties by introducing a representation in which the spins are fractionalized.

1.4.1 Slave-fermions

We will introduce the slave-fermion approach to study the Heisenberg model on the square lattice in order to discuss the main ideas behind the so-called projective construction. The slave-fermion approach in the context of $SU(2)$ spins was introduced by Baskaran *et al.* [27, 41] and was latter extended by Affleck and Marston [43] for the case of $SU(N)$ where, for $N \to \infty$, the mean-field theory of the projective construction is exact. Consider the Heisenberg antiferromagnet ($J > 0$) on the square lattice with N_s spins:

$$\mathcal{H} = J \sum_{\langle ij \rangle} \vec{S}_i \cdot \vec{S}_j \tag{1.6}$$

We start by introducing a fermionic representation of the spins:

$$\vec{S}_i = \frac{1}{2} \sum_{\alpha,\beta=\uparrow,\downarrow} c^\dagger_{i\alpha} \vec{\sigma}_{\alpha,\beta} c_{i\beta} \tag{1.7}$$

where $c_{i\uparrow}, c_{i\downarrow}$ are spin-1/2 fermionic operators and $\vec{\sigma}$ is a vector of Pauli matrices. The fermionic operators are called *spinons*. One can check that this fermionic representation

preserves the $SU(2)$ commutation relations. Substituting the latter expression in (1.6) and using the properties of the Pauli matrices, the Hamiltonian now reads:

$$\mathcal{H} = \frac{J}{2}\sum_{\langle ij\rangle}\sum_{\alpha,\beta} c^\dagger_{i\alpha}c_{j\alpha}c^\dagger_{j\beta}c_{i\beta} + J\sum_{\langle i,j\rangle}\left(\frac{1}{2}n_i - \frac{1}{4}n_i n_j\right) \tag{1.8}$$

Where $n_i \equiv c^\dagger_i c_i$. We note that this new representation enlarges the original physical Hilbert from 2^{N_s} to 4^{N_s} and thus must be supplemented with a constraint in order to correctly describe the spin degrees of freedom of (1.6). This constraint corresponds to having only one fermion per-site:

$$\sum_{\alpha=\uparrow,\downarrow} c^\dagger_{i\alpha}c_{i\alpha} = 1 \tag{1.9}$$

Under this constraint, the second term of (1.8) is just a constant and will be dropped. This new representation now allows us to use a mean-field theory in order to solve $\mathcal{H}$ by decoupling its quartic term using $\chi_{ij} = J\left\langle c^\dagger_{i\alpha}c_{j\alpha}\right\rangle/2$:

$$\mathcal{H}^{MF} = -\sum_{\alpha}\sum_{\langle ij\rangle}\left[\left(c^\dagger_{i\alpha}c_{j\alpha}\chi_{ij} + H.c.\right) - \frac{2}{J}\left|\chi_{ij}\right|^2\right], \quad \text{with} \quad \sum_{\alpha} c^\dagger_{i\alpha}c_{i\alpha} = 1 \tag{1.10}$$

We may gain a further remarkable (yet at this point still somewhat formal) insight by considering the path integral formulation of $\mathcal{H}^{MF}$ where the constraint is implemented via a time and site dependent Lagrange multiplier $\phi_i(t)$ [32]. The Lagrangian of the path integral reads [44]:

$$\mathscr{L} = \sum_{i,\alpha} c^\dagger_{i,\alpha}(i\partial_t + \mu)c_{i,\alpha} + \sum_{i,\alpha}\phi_i\left(c^\dagger_{i,\alpha}c_{i,\alpha} - 1\right) + \sum_{\langle ij\rangle}\left[\sum_{\alpha}\left(c^\dagger_{i\alpha}c_{j\alpha}\chi_{ij} + H.c.\right) - \frac{2}{J}\left|\chi_{ij}\right|^2\right] \tag{1.11}$$

This Lagrangian has a $U(1)$ gauge structure since it is invariant under:

$$c^\dagger_i \to c^\dagger_i e^{-i\theta_i}, \quad \chi_{ij} \to \chi_{ij}e^{i(\theta_i-\theta_j)}, \quad \phi_i \to \phi_i + \partial\theta_i/\partial t \tag{1.12}$$

Thus, we see that this $U(1)$ gauge structure arises[9] *as a consequence of the projective construction* (i.e. of the one fermion per site constraint) and is in fact a generic property

[9] And because this construction is meant to describe the low-energy properties of $\mathcal{H}$, this $U(1)$ gauge structure is said to be *emergent*.

of the slave-particle formulations [32]. Thus we see that gauge-theories are closely related to the description of fractionalized phases such as quantum spin liquids. As a consequence, we may hope to gain insights in the physics of the QSL by using the extensive knowledge of gauge theories. The low-energy physics of $\mathscr{L}$ corresponds to a theory of lattice fermions coupled to a $U(1)$ gauge field which is the phase of $\chi_{ij} = |\chi_{ij}| e^{iA_{ij}}$. The amplitude fluctuations of χ_{ij} are gapped and are thus not essential to the discussion.

To perform further calculations, one may as a first approximation assume a static χ_{ij} which is equivalent to searching for the saddle-point solution of $\mathscr{L}$ and neglecting gauge field fluctuations. This approximation is justified in the large-N limit where $SU(N)$ spins instead of $SU(2)$ spins are considered. In the $SU(N)$ case [43], the mean-field Hamiltonian in the slave-fermion representation reads:

$$\mathcal{H}^{MF} = -\sum_{\alpha}\sum_{\langle ij\rangle}\left[\left(c^{\dagger}_{i\alpha}c_{j\alpha}\chi_{ij} + H.c.\right) - \frac{N}{J}\left|\chi_{ij}\right|^2\right], \quad \text{with} \quad \sum_{\alpha} c^{\dagger}_{i\alpha}c_{i\alpha} = \frac{N}{2}. \tag{1.13}$$

Thus we see that for $N \to \infty$, the saddle-point approximation is exact. To lowest order in $1/N$ the allowed fluctuations involve moving only a single spinon so that for sufficiently large N, the constraint may only be implemented on average. Finally, assuming that this is qualitatively correct down to $N = 2$, one is left with solving the following theory:

$$\mathcal{H}^{MF} = -\sum_{\alpha}\sum_{\langle ij\rangle}\left[\left(c^{\dagger}_{i\alpha}c_{j\alpha}\chi_{ij} + H.c.\right) - \frac{2}{J}\left|\chi_{ij}\right|^2\right], \quad \text{with} \quad \left\langle \sum_{\alpha} c^{\dagger}_{i\alpha}c_{i\alpha} \right\rangle = 1. \tag{1.14}$$

Depending on the mean-field *ansatz* χ_{ij} which minimizes $\mathcal{H}^{MF}$, we will obtain different spin liquids. The symmetry properties of χ_{ij} constitute the basis for classifying spin liquids according to the so-called *projective symmetry group*[32]. This type of classification is however beyond the scope of this work. We will only remark that the different spin liquids phase may in part be classified by the flux that the spinons experience. Here, the flux are gauge-invariant labels that are given by the circulation of the spin ice A_{ij} on some closed contour.

We remark that the large-N approximation can be improved by generating successive terms in a $1/N$ expansion [43]. Since we are generally interesting in the case $N = 1$ or $N = 2$, such expansion may give unsatisfactory results in this limit. Thus, it seems that the analytical treatment of the slave-particle formalism would generally be uncontrolled. That being said however, this approach serves as a way to gain insight into the complicated structure of a quantum spin liquid and should be combined with the understanding provided by numerical unbiased methods such as the Density Matrix Renormalization Group

approach [45] or Quantum Monte Carlo simulations [46]. Three dimensional frustrated quantum magnets are however notoriously hard to study since in many cases of interest, no unbiased method can be used to study these systems. Indeed, DMRG cannot be used in 3 dimensional systems [45] and QMC simulations [46, 47] of frustrated systems are often plagued by the infamous sign problem. One then has to rely on biased methods such as the slave-particle treatment.

Despite the aforementioned drawbacks, the virtue of slave-particle approaches perhaps best reside in the fact that it may give insights in the form of the quantum spin liquid wave-function that the system selects. One's hope is that in solving Hamiltonian $\mathcal{H}^{MF}$, the essential qualitative physics of the QSL may be extracted. It is in fact possible to exactly take into account the constraint required to project back to the physics Hilbert space via the so-called Gutzwiller projection method [48]. The idea behind this approach is to start from variational wave-function $|\psi(\{\alpha\})\rangle$ which, for some restricted set of variational parameters, constitute the exact ground state of the mean-field Hamiltonian in the slave-particle formulation. Then by explicitly projecting out the unphysical part of that wave-function (zero or two fermion per-site states) via a projector of the form:

$$|\psi_{\text{spin}}\rangle = \mathscr{P}_{GW}\,|\psi(\{\alpha\})\rangle \qquad \mathscr{P}_{GW} = \prod_i \left(c_i^\dagger\,|0\rangle\langle 0|\,c_i\right) \tag{1.15}$$

one obtains a physical spin-wave function $|\psi_{\text{spin}}\rangle$. Finally, using the proper normalization of $|\psi_{\text{spin}}\rangle$, one then computes a variational energy:

$$E(\{\alpha\}) = \frac{\langle\psi_{\text{spin}}|\,\mathcal{H}\,|\psi_{\text{spin}}\rangle}{\langle\psi_{\text{spin}}|\psi_{\text{spin}}\rangle}, \tag{1.16}$$

which is then minimized with respect to the set of variational parameters $\{\alpha\}$. Generally, the latter expression is computed via a Monte Carlo procedure since it becomes rapidly computationally expensive to compute matrix elements as the size of the system is increased.

1.5 Quantum spin ice

Motivated by the rich possibilities of QSL and their corresponding emergent of gauge theories, we now discuss the main subject of this thesis: quantum spin ice. Already, we have seen that classical spin ice has a remarkable correspondence with electromagnetism. A natural question to ask is what are the effects of quantum fluctuations in a spin ice system. This question was originally studied by Hermele *et al.* [2] for the case of the $S = 1/2$ XXZ model with global $U(1) \otimes \mathbb{Z}_2$ symmetry on the pyrochlore lattice:

$$\mathscr{H}_{\text{XXZ}} = J_{zz} \sum_{\langle ij \rangle} S_i^z S_j^z - J_{\pm} \sum_{\langle ij \rangle} \left(S_i^+ S_j^- + S_i^- S_j^+ \right), \tag{1.17}$$

with $0 < J_{\pm} \ll J_{zz}$[10]. The effect of the $J_{\pm}$ term on a spin ice state is simple: either it creates a pair of spinons or hops a spinon (see Fig. 1.8). Hermele *et al.* used degenerate

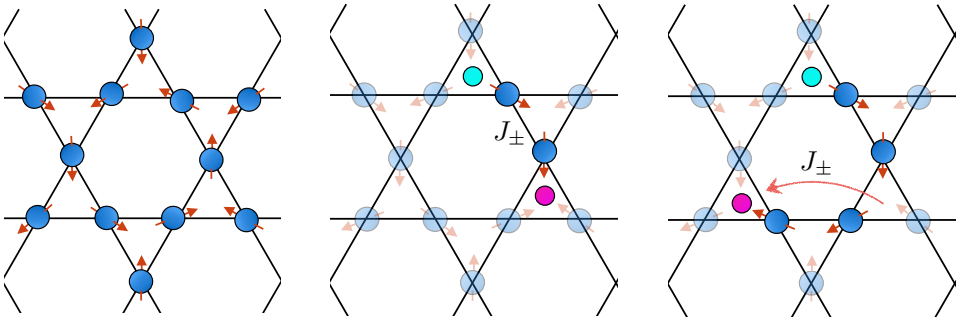

Figure 1.8: (Left figure) One of the [111] kagome plane of the pyrochlore lattice in a projected spin ice configuration. The $J_{\pm}$ term may create a pair of spinons (middle figure) or move spinon around (right figure).

perturbation theory in the spin ice manifold to derive an effective Hamiltonian for Eq. (1.17) which, to lowest order, assumes the following form:

$$\mathcal{H}_{\text{eff}} = -\frac{3J_{\pm}^3}{2J_{zz}^2} \sum_{\hexagon} \left(S_1^+ S_2^- S_3^+ S_4^- S_5^+ S_6^- + H.c. \right) + \text{const.}, \tag{1.18}$$

where the spins belong to the same hexagonal plaquette. The sum is carried over all hexagonal plaquettes (see Fig. 1.2) on the pyrochlore lattice. This Hamiltonian describes

[10] Denoting the energy scale of the quantum fluctuations by $J_{\perp}$, we will hereafter refer to quantum spin ice (or the quantum spin ice regime) as the $|J_{\perp}| \lesssim J_{zz}$ regime (with $J_{zz} > 0$).

the dispersion of the spin ice manifold to lowest order in $J_\pm$ (see Fig. 1.9). Since it describes only the spin ice manifold, it also possesses a $U(1)$ gauge structure which arises because of the charge conservation constraint. The $U(1)$ gauge structure is generated by the charge on every tetrahedron:

$$Q_{\boldsymbol{x}} = \eta_{\boldsymbol{x}} \sum_{\mu=0}^{3} S^z_{\boldsymbol{x}\mu}. \tag{1.19}$$

The spin ice constraint translates to $Q_{\boldsymbol{x}} = 0 \ \forall \ \boldsymbol{x}$ and we see that $[Q_{\boldsymbol{x}}, \mathcal{H}_{\mathit{eff}}] = 0 \ \forall \ \boldsymbol{x}$. Furthermore, this effective Hamiltonian is equivalent to a hard-core dimer model on the diamond lattice [2]. This is seen by considering $S^z_{\boldsymbol{x}\mu} = +1/2$ ($S^z_{\boldsymbol{x}\mu} = -1/2$) to be the presence (absence) of a dimer on the link $\langle \boldsymbol{x}, \boldsymbol{x} + \eta_{\boldsymbol{x}} \mathbf{e}_\mu \rangle$. The $Q_{\boldsymbol{x}} = 0$ constraint then becomes the constraint that every diamond site is "touched" by two dimers [2].

The effective theory can be described by a compact $U(1)$ gauge theory in its deconfined phase, by leveraging the extensive knowledge of the properties of the quantum dimer model [49, 50, 51, 52]. Both the quantum ground state and its gapless gauge fluctuations corresponding to photons are coherent superpositions of classical spin ice configurations. The predicted $U(1)$ liquid was later found by a quantum Monte-Carlo study [53] of the XXZ model at finite temperature. The properties of the spin liquid have been further characterized in detail by both analytical investigations and quantum Monte-Carlo simulations [23, 54] of the dimer model at $T = 0$.

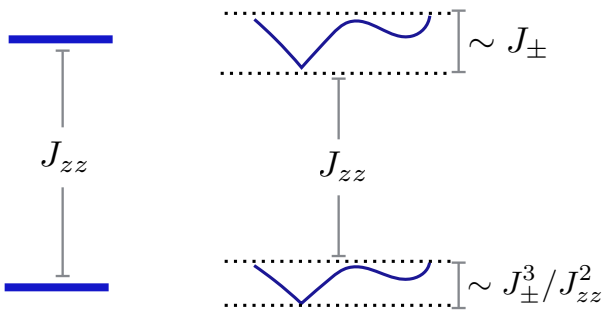

Figure 1.9: (Left) The ground state and first excited state manifolds of classical spin ice. (Right) To lowest order the $J_\pm$ creates a dispersion with bandwidth $\sim J_\pm^3/J_{zz}^2$ in the ground state manifold and also disperses the spinons.

1.5.1 Quantum spin ice as a realistic model

The remarkable properties of the XXZ model are interesting to study in their own right, but one may wonder if the $S = 1/2$ quantum spin ice is a realistic model in an experimental setting. Here we will briefly review the phenomenology that leads to the description of some rare-earth pyrochlore oxides in terms of an anisotropic $S = 1/2$ model.

In the past decade there has been numerous experimental studies on the rare-earth pyrochlore oxides ($R_2B_2O_7$) [55]. In these compounds, the spin-orbit interaction of the f electrons of the magnetic rare-earth ion is large and the total angular moment $\vec{J} = \vec{L} + \vec{S}$ is a good quantum number. Hund's rules can than be applied to determine the electronic ground state of the isolated magnetic ions. The local (quasi) octahedral crystalline environment (due to the oxygens ions) of the rare-earth ions induces a crystal field which lift the degeneracy of the $2J + 1$ degenerated ground state. If the number of electrons in the outer partially filled f orbital is odd, then Kramers theorem guarantees that the ground state is at least two-fold degenerate. Moreover, if the first excited doublet is well separated from the ground state doublet (with a gap much larger than the inter-ion interactions), then the essential low-energy physics of rare-earth ions is encoded in an effective Kramers doublet (i.e. a $S = 1/2$ model) model on the pyrochlore lattice. Finally, if these Kramers doublet transforms like magnetic dipole (i.e. as pseudovectors) under space group symmetries, then using group theoretical arguments [56] it is possible to show that the most general $S = 1/2$ nearest-neighbour bilinear exchange Hamiltonian on the pyrochlore lattice (and in local coordinate) reads:

$$\mathcal{H} = J_{zz} \sum_{\langle ij \rangle} S_i^z S_j^z - J_{\pm} \sum_{\langle ij \rangle} \left(S_i^+ S_j^- + H.c. \right) \tag{1.20}$$

$$+ J_{\pm\pm} \sum_{\langle ij \rangle} \left(\gamma_{ij} S_i^+ S_i^+ + H.c. \right) + J_{z\pm} \sum_{\langle ij \rangle} \left(\zeta_{ij} \left[S_i^z S_j^+ + S_j^z S_i^+ \right] + H.c. \right), \tag{1.21}$$

where ζ, γ are unimodular matrices (with $\zeta = -\gamma^\star$) that encode the cubic symmetry of the pyrochlore lattice [57] and that are given in Appendix A. Interestingly, recent theoretical work has pointed out the possibility to realize a simpler model in systems where the transverse components of the Kramers doublets transform as a component of the magnetic octupolar tensor [33]. In this setting the effective model obtained is a surprisingly simple XYZ (with global $\mathbb{Z}_2 \otimes \mathbb{Z}_2 \otimes \mathbb{Z}_2$ symmetry) model.

A useful property of the rare-earth pyrochlore oxides is that they posses a strong single-ion magnetic moment. For instance $Yb_2Ti_2O_7$ and $Er_2Ti_2O_7$ have respectively a paramagnetic moment of $\mu \approx 3.34\mu_B$ [58] and $\mu \approx 3.8\mu_B$ [59]. Thus it has been possible to study these materials in a ferromagnetic state obtained at low-temperatures with

the application of a modest (on the order of 5 Teslas) magnetic field [57, 60]. Using inelastic neutron scattering in this regime, multiple sharp spin-wave branches were measured and subsequent spin-wave calculations with model (1.21) were made in order to fit the $\{J_{zz}, J_{\pm}, J_{\pm\pm}, J_{z\pm}\}$ exchange parameters to the experimental measurements. As expected[11] for $Er_2Ti_2O_7$, the estimation of the exchange couplings for this compound indicates that it is not a quantum spin ice. The estimation of the couplings for $Yb_2Ti_2O_7$ on the other hand indicates that it is a quantum spin ice with $(J_{zz}, J_{\pm}, J_{\pm\pm}, J_{z\pm}) = (0.17 \pm 0.04, 0.05 \pm 0.01, 0.05 \pm 0.01, -0.14 \pm 0.01)$[57]. Further numerical investigations using model (1.21) and the estimated exchange coupling where carried in order to compute the specific heat for $Yb_2Ti_2O_7$. This study indicates a good agreement between the numerical results and the experimental measurements [64].

A number of other compounds are thought to be potential quantum spin ice candidates. These include $Pr_2Zn_2O_7$, $Pr_2Sn_2O_7$ and $Tb_2Ti_2O_7$ [24]. The latter compound is the first compound that has been proposed as a quantum spin ice candidate [65, 66, 67]. In the recent work of Ref.[68], the exchange parameters for $Tb_2Ti_2O_7$ were estimated to be $(j_{\pm}, j_{\pm\pm}, j_{z\pm}) = (-1.1, -1.25, -0.92)$ in units of $J_{zz} = 1$.

Finally, we merely remark that for all of these quantum spin ice candidates, the experimental measured low-temperature is a matter of hot debate [24]. This may be an indication that some exotic physics is at play in these compounds.

[11] $Er_2Ti_2O_7$ behaves like a an unfrustrated magnets althought, interestingly, studies have put forward multiple evidences that the ordered phase of $Er_2Ti_2O_7$ is selected by cooperative thermal and quantum fluctuations [60, 61, 62, 63].

Chapter 2

Model and Method

2.1 A projective construction for quantum spin ice

The gauge theory that arises for the effective Hamiltonian described in section 1.5 does not include the effect of charged matter fields (or electric charges) and their coupling with the compact $U(1)$ spin ice. Recently, a novel gauge theory formulated in terms of slave-rotors was introduced by Savary *et al.* [3, 69] in order to establish the regime of stability of the Coulomb phase from which they obtained a phase diagram (see Fig. 2.1). Here we partially reproduce and discuss some new aspects of their theory that were discussed before.

We start our discussion from the XXZ model (1.17) in terms of the diamond lattice coordinates:

$$\mathscr{H}_{\text{XXZ}} = J_{zz} \sum_{\boldsymbol{x}} \sum_{\mu<\nu} S^z_{\boldsymbol{x}\mu} S^z_{\boldsymbol{x}\nu} - J_{\pm} \sum_{\boldsymbol{x}} \sum_{\mu<\nu} \left(S^+_{\boldsymbol{x}\mu} S^-_{\boldsymbol{x}\nu} + H.c. \right) + \text{const.}, \tag{2.1}$$

Moreover, from now on and hereafter, we take $J_{zz} = 1$ and denote the other scaled interactions by a lower case $J_{\pm} \to j_{\pm}$, etc.

Following Ref. [3], on each diamond lattice site we now introduce the following conjugate rotor variables $\hat{\theta}_{\boldsymbol{x}}$ and $\hat{Q}_{\boldsymbol{x}}$[1], that satisfy:

$$\left[\hat{\theta}_{\boldsymbol{x}}, \hat{Q}_{\boldsymbol{x}'} \right] = i\delta_{\boldsymbol{x},\boldsymbol{x}'}. \tag{2.2}$$

[1]Note here that the charge $Q_{\boldsymbol{x}}$ introduced before is related to this rotor variable via a constraint.

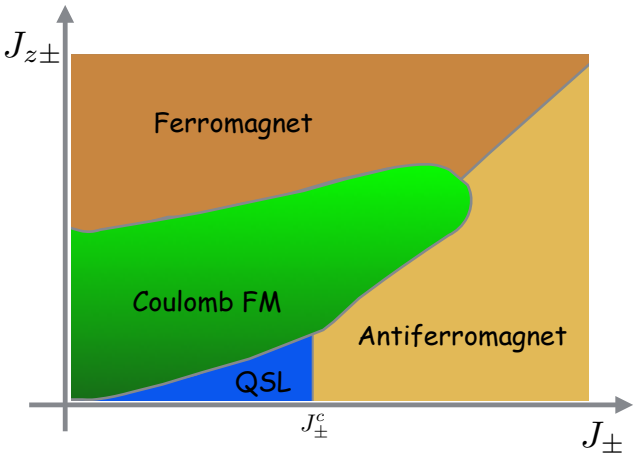

Figure 2.1: Reproduction of the phase diagram obtained by Savary *et al.* in the context of a gauge mean-field theory study of Hamiltonian (1.21) with $J_{\pm\pm} = 0$. They found that two exotic phases are realized over a finite extent of the phase diagram : a $U(1)$ quantum spin liquid (QSL) and a "Coulomb ferromagnet" [3]. The latter phase has fully ordered moments while (remarkably) still supporting deconfined spinons. Along the $J_{z\pm} = 0$ line, the QSL phase becomes unstable around $J_\pm^c \approx 0.192 J_{zz}$.

The charge operator $\hat{Q}_{\boldsymbol{x}}$ has an associated raising operator $\psi_{\boldsymbol{x}}^\dagger = e^{i\hat{\theta}_{\boldsymbol{x}}}$ which obeys:

$$\left[\psi_{\boldsymbol{x}}, \hat{Q}_{\boldsymbol{x}'}\right] = \psi_{\boldsymbol{x}} \delta_{\boldsymbol{x}\boldsymbol{x}'}. \tag{2.3}$$

Thus, $\psi_{\boldsymbol{x}}$ decreases the charge at site $\boldsymbol{x}$ by one and $\psi_{\boldsymbol{x}}^\dagger$ increases the charge at site $\boldsymbol{x}$ by one: $\psi^\dagger |Q\rangle = |Q+1\rangle$. The transverse component of the spins ($S_{\boldsymbol{x}\mu}^\pm$) are represented using rotor variables combined with pseudo-spin operators (s^+):

$$S_{\boldsymbol{x}\mu}^+ = \psi_{\boldsymbol{x}}^\dagger s_{\boldsymbol{x}\mu}^+ \psi_{\boldsymbol{x}+\mu}, \quad S_{\boldsymbol{x}\mu}^- = \psi_{\boldsymbol{x}+\mu}^\dagger s_{\boldsymbol{x}\mu}^- \psi_{\boldsymbol{x}}, \quad \boldsymbol{x} \in \langle a \rangle \,. \tag{2.4}$$

The new variables $(s^\pm, \psi)$ live in the enlarged Hilbert space $H_{\text{big}} = \left(\bigotimes_i H_{1/2}\right) \otimes \left(\bigotimes_{\boldsymbol{x}} H_Q\right)$, where $\bigotimes_i H_{1/2}$ denotes the Hilbert space of the pseudo-spin $(s^\pm, s^z)$, i.e. in the s^z basis it is spanned by $\{|\uparrow\rangle, |\downarrow\rangle\}$ on every diamond lattice bonds (or equivalently every pyrochlore lattice site). The $\bigotimes_{\boldsymbol{x}} H_Q$ corresponds to the Hilbert space of the rotors and is spanned by $\{|Q\rangle\}$ with $Q = 0, \pm 1, \pm 2, \cdots$ on every diamond lattice site. The original Hilbert space is exactly recovered by restricting $|Q|$ to take integer values $0, 1$ or 2. This constraint is

implemented by requiring that:

$$\hat{Q}_{\boldsymbol{x}} = \sum_{\mu=0}^{3} S^z_{\boldsymbol{x}\mu} \tag{2.5}$$

We now express the spin ice exchange term of Eq. (2.1) using $\hat{Q}_{\boldsymbol{x}}$:

$$\hat{Q}^2_{\boldsymbol{x}} = \sum_{\substack{\mu,\nu \\ \mu\neq\nu}} S^z_{\boldsymbol{x}\mu} S^z_{\boldsymbol{x}\nu} + \text{const.} \quad , \tag{2.6}$$

and take the classical spin ice energy (for which $Q_{\boldsymbol{x}} = 0$ and $J_\pm = 0$) to be zero by dropping the additional constant. The XXZ Hamiltonian in terms of the rotor variables now reads:

$$\mathscr{H}_{\text{XXZ}} = \sum_{\boldsymbol{x}} \frac{\hat{Q}^2_{\boldsymbol{x}}}{2} - j_\pm \sum_{\boldsymbol{x}\in\langle a\rangle} \sum_{\mu<\nu} \psi^\dagger_{\boldsymbol{x}+\mu} \psi_{\boldsymbol{x}+\nu} s^+_{\boldsymbol{x}\nu} s^-_{\boldsymbol{x}\mu} + \psi^\dagger_{\boldsymbol{x}} \psi_{\boldsymbol{x}+\mu-\nu} s^+_{\boldsymbol{x}\mu} s^-_{\boldsymbol{x}+\mu-\nu,\nu} + H.c. \tag{2.7}$$

Note that constraint $|Q| \leq 2$ will not be implemented explicitly in the subsequent calculations but will emerge dynamically in the range of validity of the theory (i.e where J_{zz} is the largest interaction)[70].

2.1.1 Lattice quantum electrodynamics with matter fields

In order to have a more transparent relation to quantum electrodynamics, the Ising components are interpreted as electric-field variables (as discussed in section 1.2.1): $S^z_{\boldsymbol{x}\mu} = s^z_{\boldsymbol{x}\mu} \equiv E_{\boldsymbol{x}\mu}$[2]. Moreover, we introduce a gauge field link variable $A_{\boldsymbol{x}\mu}$, conjugate to the electric-field:

$$[A_{\boldsymbol{x}\mu}, E_{\boldsymbol{x}'\nu}] = i\delta_{\boldsymbol{x}\boldsymbol{x}'}\delta_{\mu\nu}. \tag{2.8}$$

Then, $s^\pm$ becomes the raising/lowering operator for $E_{\boldsymbol{x}\mu}$:

$$s^\pm_{\boldsymbol{x}\mu} \to e^{\pm iA_{\boldsymbol{x}\mu}} \tag{2.9}$$

In using such a representation for $s^\pm$, we see that we have again enlarged our Hilbert space and $E_{\boldsymbol{x}\mu}$ may now take any half-integer value. In order to constrain $E_{\boldsymbol{x}\mu} = \pm 1/2$ we will explicitly add a new term to our theory which we discuss below.

[2]Since $S^z_{\boldsymbol{x}\mu} = s^z_{\boldsymbol{x}\mu}$ are both the z component of $S = 1/2$ spin operators, we do not distinguish them.

The new representation admits a compact[3] $U(1)$ gauge structure with:

$$A_{\boldsymbol{x}\mu} \to A_{\boldsymbol{x}\mu} + \alpha_{\boldsymbol{x}} - \alpha_{\boldsymbol{x}+\mu}, \qquad \psi_{\boldsymbol{x}} \to \psi_{\boldsymbol{x}} e^{i\alpha_{\boldsymbol{x}}}, \tag{2.10}$$

such that the physical spin, $S^{\pm}_{\boldsymbol{x}\mu}$, remains invariant under this gauge transformation. Thus, substituting the representation Eq. (2.4) and Eq. (2.9) into the XXZ model defined in Eq. (2.1), we obtain a compact $U(1)$ gauge theory:

$$\mathscr{H}_{U(1)} = \sum_{\boldsymbol{x}} \frac{\hat{Q}^2_{\boldsymbol{x}}}{2} - \frac{j_{\pm}}{4} \sum_{\boldsymbol{x}\in\langle a\rangle} \sum_{\mu<\nu} \psi^{\dagger}_{\boldsymbol{x}+\mu}\psi_{\boldsymbol{x}+\nu} e^{i(A_{\boldsymbol{x}\nu} - A_{\boldsymbol{x}\mu})} + \psi^{\dagger}_{\boldsymbol{x}}\psi_{\boldsymbol{x}+\mu-\nu} e^{i(A_{\boldsymbol{x}\mu} - A_{\boldsymbol{x}+\mu-\nu,\nu})} + H.c. \tag{2.11}$$

$$+ U \sum_{\boldsymbol{x}\in\langle a\rangle} \sum_{\mu} (E^2_{\boldsymbol{x},\boldsymbol{x}+\mu} - \frac{1}{4}) \tag{2.12}$$

Compared with the Hamiltonian studied in Ref. [3], we have added Eq. (2.12). The term proportional to U controls the dynamics of the gauge field as it is the case in standard electrodynamics $\mathbf{E} \sim \partial\mathbf{A}/\partial t$. This term is introduced in a large-N approximation (similarly to what is done in the slave-fermion formulation addressed in section 1.4.1) to enforce the $E_{\boldsymbol{x}} = \pm 1/2$ constraint on average. As discussed earlier, a rigorous treatment of this constraint requires more involved calculations that we will not delve into in this presentation. This analysis is left for further work.

Although U is to be determined by requiring that $\langle E^2_{\boldsymbol{x}}\rangle = 1/2$, we also remark that the limit $U \to \infty$ is non-trivial as opposed to the conventional lattice QED [22]. This is to be contrasted with the case where $E_{\boldsymbol{x}\mu}$ would take integer values and where $U \to \infty$ would yield to a trivial limit with $E_{\boldsymbol{x}\mu} = 0$ everywhere. For this reason, the gauge-theory discussed above is said to be a frustrated gauge theory [2, 22].

The operator $s^{\pm}$ is not a physical spin but should be interpreted as a gauge field operator. We see that with the representation (2.4), the effect of $j_{\pm}$ discussed in Fig. 1.8 is reproduced. Indeed, in $\mathscr{H}_{U(1)}$, $\psi^{\dagger}_{\boldsymbol{x}+\mu}\psi_{\boldsymbol{x}+\nu}$ hops a charge from diamond site $\boldsymbol{x}+\nu$ to $\boldsymbol{x}+\mu$ in the background of an effective gauge-invariant magnetic field which corresponds to the circulation of the gauge fields around closed loops (see below).

Further insights may be obtained by substituting the rotor representation Eq. (2.4),(2.9) in the effective model derived by Hermele *et al.* (see Eq. 1.18):

$$\mathcal{H}_{\text{eff}} \to -\frac{3j^3_{\pm}}{2} \sum_{\hexagon} \cos(A_1 - A_2 + A_3 - A_4 + A_5 + A_6) + U \sum_{\boldsymbol{x}\in\langle a\rangle} \sum_{\mu} (E^2_{\boldsymbol{x},\boldsymbol{x}+\mu} - \frac{1}{4}), \tag{2.13}$$

[3]The compactness is just a consequence of the fact that the gauge charge $Q_{\boldsymbol{x}}$ is quantized [22].

where the A_i correspond to the gauge fields that live on the links of the hexagonal plaquettes of the diamond lattice. Eq. (2.13) determines the static part of the gauge fields at the lowest order in $j_\pm$ (using $U = 0$, Eq. (2.13) becomes a classical model). Again, because we use the representation $s^+ = e^{iA}$, we have included a constraint on $E_{\boldsymbol{x},\boldsymbol{x}\mu}$ via the $E^2_{\boldsymbol{x},\boldsymbol{x}\mu}$ term. We can further define a circulation around a particular loop C as follow:

$$B_C = \sum_{(\boldsymbol{x},\boldsymbol{x}\nu)\in\ C} \eta_{\boldsymbol{x}} A_{\boldsymbol{x},\boldsymbol{x}\nu}, \tag{2.14}$$

and we see that for $j_\pm > 0$, with the assumption[4] that $U \ll j_\pm^3$, $\mathcal{H}_{\text{eff}}$ assumes the familiar form:

$$\mathcal{H}_{\text{eff}} \to -\frac{3j_\pm^3}{2} \sum_{\hexagon} \cos(B_{\hexagon}) + U \sum_{\boldsymbol{x}\in\langle a\rangle} \sum_{\mu} E^2_{\boldsymbol{x},\boldsymbol{x}+\mu} + \text{const.} \tag{2.15}$$

$$\xrightarrow{j_\pm>0} \frac{3j_\pm^3}{4} \sum_{\hexagon} B^2_{\hexagon} + U \sum_{\boldsymbol{x}\in\langle a\rangle} \sum_{\mu} E^2_{\boldsymbol{x},\boldsymbol{x}+\mu} + \text{const.} + \mathcal{O}(B^4_{\hexagon}) \tag{2.16}$$

where we recognize the quantum electrodynamics (without matter fields) Hamiltonian. The speed of light is given by [23]:

$$c = \sqrt{\frac{3j_\pm^3}{4} U}. \tag{2.17}$$

In going from Eq. (2.15) to Eq. (2.16), we have considered the case $0 < j_\pm \ll 1$, where a magnetic flux $B_{\hexagon} \approx 0$ for every hexagonal plaquette is expected. We see that in this limit, the compactness of the gauge fields is not important. The full effective theory (Eq. (2.13)) however is a compact $U(1)$ gauge theory which implies that quantized magnetic charges may also be present in the ground state [2]. These charges live at the center of the cell formed by the four hexagonal plaquettes of the pyrochlore lattice unit cell (see Fig. 2.2). In subsequent sections we will use this fact to guide our choice in determining different *ansatz* for the static part of the gauge fields.

In the limit where $U \to \infty$, the theory remains none trivial (as mentioned above). We will refer to the $U = 0$ limit as the limit where the gauge-field are static.

[4] We will see later that this assumption is, on the basis of quantum Monte Carlo results [54], not entirely justified.

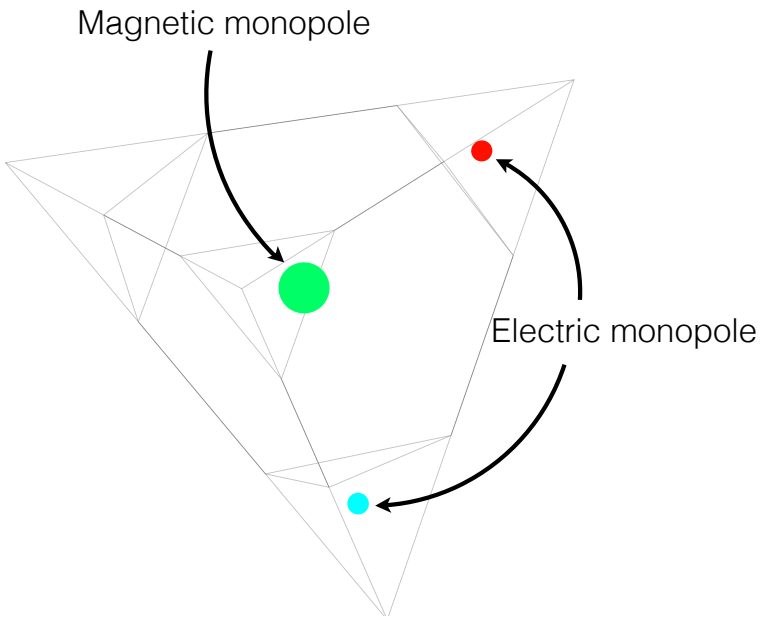

Figure 2.2: The magnetic charge (green sphere) or magnetic "monopole" of the compact $U(1)$ gauge theory lives at the center of the unit cell formed by four hexagonal plaquette. The electric charges of the theory are represented as red and cyan spheres.

2.2 Gauge mean-field theory

Quantum Monte Carlo simulations have demonstrated the existence of a deconfined phase where the spinons are free to propagate [23, 53]. To go further in our analytical treatment, we perform a mean-field treatment for the lattice gauge theory of Eq.(2.11) [71]. This can be achieved by first fixing the gauge and then dealing with the remaining global $U(1)$ symmetry which can in turn be spontaneously broken [72]. In the present case, the global $U(1)$ symmetry corresponds to the conservation of charge on both diamond sublattices, $\langle a \rangle$ and $\langle b \rangle$, taken separately. Spontaneously breaking this $U(1)$ global symmetry is equivalent to the condensation of the charged matter fields into a superfluid phase which in turns leads to a screening of the electric flux and a generation of a mass for the gauge fields: this is the Higgs mechanism [73]. Thus, the region of stability of the $U(1)$ liquid phase is bounded by the points at which the spinon condenses. As we briefly explain it below, confined phases (where fractionalized excitations are absent of the spectrum) and Higgs phases may or may not be smoothly connected.

2.2.1 Phases in gauge theories with matter fields

In a $U(1)$ lattice gauge theory with matter fields we may distinguish three general type of phases that may arise [4]:

1. Higgs phases: Higgs mechanism leads to a mass for the photons and short-ranged interaction amongst static matter fields. In the spin language, this corresponds to a long-range ordered phase with no exotic excitations.

2. Coulomb phase: Photons are massless and give rise to a Coulomb-like interaction amongst the matter fields. There are massive free charges in the spectrum.

3. Confined phases: The photons are massive and there are no free charges in the spectrum. In the spin language, this corresponds to a long-range ordered phase with no exotic excitations.

In some cases (as for the one discussed in this thesis), the confined phase and the Higgs phases may be distinguished on symmetry grounds (see Table 2.1 and we refer the reader to Ref. [73] for a more thorough discussion about how these phases may or may not be related).

2.2.2 Pure compact $U(1)$ gauge theory

The compact nature of the gauge-fields automatically implies that it's flux is quantized [74]. According to Gauss's theorem, this flux is equal to the charges that act a sources. Thus, the charges are automatically quantized in a compact gauge theory [74]. In the case of the abelian $U(1)$ gauge theory in $d = 2$ *spatial* dimensions, it can be shown that the theory is always confined due to instanton effects. Instanton corresponds to the tunelling between different configurations that locally minimize the action of the system. In $d = 2$, there is a finite density of instantons (at all coupling strength) interacting at long distances which leads to a confinement of the charges. It turns out that this results also holds true for non-abelian gauge theories $d = 2$. In $d = 3$, it turns out that depending on the coupling strength, the vacuum state of the system may or may not be filled with a condensate of magnetic monopoles (which were instantons in $d = 2$). Thus depending on the coupling strength, the system may or may not be confined [74].

2.2.3 Sectors of quantum spin ice

We now seperate the gauge field $A_{\boldsymbol{x}\mu}$ into a static part, $\bar{A}_{\boldsymbol{x}\mu}$, and a fluctuating part, $\tilde{A}_{\boldsymbol{x}\mu}$:

$$A_{\boldsymbol{x}\mu} = \bar{A}_{\boldsymbol{x}\mu} + \tilde{A}_{\boldsymbol{x}\mu}. \tag{2.18}$$

The choice for $\bar{A}_{\boldsymbol{x}\mu}$ will be guided by a perturbative treatment of the original Hamiltonian. The perturbative result for XXZ quantum spin ice is to lowest order given by Eq. (1.18). In the following chapter we will address the effect of the terms generated to fourth and fifth order in degenerate perturbation theory. All in all, with Eq. (2.18), the Hamiltonian (2.11) splits into three terms:

$$\mathscr{H}_{U(1)} = \mathscr{H}_{\mathrm{s}}(\hat{Q}_{\boldsymbol{x}}, \psi_{\boldsymbol{x}}) + \mathscr{H}_{\mathrm{g}}(E_{x\mu}, \tilde{A}_{\boldsymbol{x}\mu}) + \mathscr{H}_{\mathrm{int}}(E_{\boldsymbol{x}\mu}, \tilde{A}_{\boldsymbol{x}\mu}, \psi_{\boldsymbol{x}}) \tag{2.19}$$

where $\mathscr{H}_{\mathrm{s}}$ and $\mathscr{H}_{\mathrm{g}}$ correspond respectively to the spinon and the gauge field sectors and where $\mathscr{H}_{\mathrm{int}}$ contains the terms that couple the two sectors. In the next chapter we will focus on describing the physics of the spinon sector ($\mathscr{H}_{\mathrm{s}}$) for both $j_{\pm} > 0$ and $j_{\pm} < 0$. The physics of $\mathscr{H}_{\mathrm{g}}$ has been addressed on phenomenological grounds in works by Benton et *al.* [23]. The role of the interaction between the gauge-field and the spinons [23] is left for future work.

2.2.4 Order parameters and phases

The different possible phases that may arise are identified by different order parameters. The $U(1)$ QSL liquid phases are distinguished by their flux patterns $\{B_c\}$ (which we will more thoroughly discuss in the following Chapter). Table 2.1 describes the different phases that may be supported by the full anisotropic theory (with $J_{\pm\pm}$ and $J_{z\pm}$). In table 2.1 the $U(1)$ liquids may be referred to as Coulomb phases where there exist massless gauge bosons (corresponding to the collective fluctuation of the gauge fields or photons) and massive electric charges (i.e. the spinons) [73]. In the Coulomb phases, the charges are uncondensed $\langle\psi\rangle = 0$ and the global $U(1)$ symmetry remains unbroken [4]. Confined phases correspond to the case where the spinons cannot propagate, i.e. where $\langle s^+\rangle = 0$. In this case, the gauge fluctuations are strong and long range order is developed along the local z-component of the spins $\langle s^z\rangle \neq 0$ [4]. Finally, we note that a $\mathbb{Z}_2$ liquid in which the $U(1)$ gauge structure is broken down to a $\mathbb{Z}_2$ structure is also possible [4] within the g-MFT description.

	$\lvert B_c\rvert$	$\langle\psi^\dagger_{\boldsymbol{x}}\psi_{\boldsymbol{x}\pm\mu}\rangle$	$\langle s^\pm\rangle$	$\langle\psi^\dagger\rangle$	$\langle s^z\rangle$	$\langle\psi^\dagger_{\boldsymbol{x}}\psi^\dagger_{\boldsymbol{x}}\rangle$
$U(1)$ liquid						
zero-flux	0	0	$\neq 0$	0	0	0
π-flux	π					
"monopole"-flux	$\pi/2$					
"spin ice"-flux	$\pi/2$					
CFM		$\neq 0$	$\neq 0$	0	$\neq 0$	0
$\mathbb{Z}_2$ liquid		0	$\neq 0$	0	0	$\neq 0$
Higgs phases		$\neq 0$	$\neq 0$	$\neq 0$	$\neq 0$	$\neq 0$
Confined phases		0	0	0	$\neq 0$	0

Table 2.1: Summary of the different possible phases within the gauge mean-field theory. The $U(1)$ liquids are distinguished by their flux $\lvert B_c\rvert$ which are explicitly given in Chapter 3. CFM refers to a Coulomb ferromagnet and Higgs phases (corresponds to classical orders) such as the ferromagnetic and antiferromagnetic are grouped in the same category.

2.3 Summary

In this Chapter we have established and discussed the framework of gauge mean-field theory introduced by Savary *et al.* [3] to map the original XXZ quantum spin ice model to a compact $U(1)$ lattice gauge theory. In the first part of the next chapter, we will study the matter sector of the theory for $j_\pm > 0$ and $j_\pm < 0$. The dispersion of the spinons will be discussed and the possibility for new exotic spin liquids will be studied via different approximation scheme. In particular we will introduce a novel representation of the quantum XY rotors in terms of "exclusive" bosons and perfom exact diagonalization on small clusters. A stability diagram for the $U(1)$ liquids found for the XXZ quantum spin ice is obtained and discussed.

Chapter 3

XXZ quantum spin ice

In the gauge mean-field approximation, the spinon sector (first term of Eq. (2.19)) assumes the form:

$$\mathscr{H}_{\mathrm{s}}(\hat{Q}_{\boldsymbol{x}}, \psi_{\boldsymbol{x}}) = \sum_{\boldsymbol{x}} \frac{\hat{Q}_{\boldsymbol{x}}^2}{2} - \frac{j_\pm}{4} \sum_{\boldsymbol{x}\in\langle a\rangle} \sum_{\mu<\nu} \psi^\dagger_{\boldsymbol{x}+\mu}\psi_{\boldsymbol{x}+\nu} e^{i(\bar{A}_{\boldsymbol{x}\nu}-\bar{A}_{\boldsymbol{x}\mu})} + \psi^\dagger_{\boldsymbol{x}}\psi_{\boldsymbol{x}+\mu-\nu} e^{i(\bar{A}_{\boldsymbol{x}\mu}-\bar{A}_{\boldsymbol{x}+\mu-\nu,\nu})} + H.c, \tag{3.1}$$

where $\bar{A}_{\boldsymbol{x}\nu}$ is a classical number and corresponds to the static part of the gauge-field. We will now analyze the case where $j_\pm > 0$ and $j_\pm < 0$ separately. The latter case corresponds to the fully frustrated XXZ quantum spin ice where the transverse components S^+S^- are frustrated. The analysis for $j_\pm < 0$ will require additional care in choosing the $\bar{A}_{\boldsymbol{x}\nu}$ configurations. Our main goal in the follow sections will be to solve Eq. (3.1) (i.e. obtain the spectrum and compute expectations values in the ground-state for different $j_\pm$) using different approximation schemes in order to derive the ground-state of the theory.

3.1 Unfrustrated XXZ quantum spin ice ($j_\pm > 0$)

Guided by the perturbative results of (2.13), we assume that the background gauge field $\bar{A}$ leads to zero magnetic fluxes through all hexagonal plaquettes when $j_\pm > 0$ [2, 3]. We are free to choose a gauge such that $\bar{A}_{\boldsymbol{x}\mu} = 0$ for all bonds $\langle \boldsymbol{x}\mu\rangle$. To demonstrate that this is possible, we consider a pyrochlore lattice of $4V$ sites. There are $4V$ $\bar{A}_{\boldsymbol{x}\mu}$ fields. As for any vector fields, $\bar{A}_{\boldsymbol{x}\mu}$ can be separated into a longitudinal part and a transverse part. The transverse contributions are magnetic fluxes through $2V$ hexagonal plaquettes related to

$\bar{A}_{\boldsymbol{x}\mu}$ by the lattice version of Stokes' theorem. These fluxes are chosen to be zero since the static part of the gauge fields is described by (recall the previous result):

$$\mathcal{H}_{\text{eff}} = -\frac{3j_{\pm}^3}{2}\sum_{\hexagon}\cos(B_{\hexagon}) \tag{3.2}$$

The remaining $2V$ longitudinal components can be fixed to be zero by tuning $2V$ $\alpha_{\boldsymbol{x}}$ (see Eq. (2.10)). We will hereafter refer to this gauge-choice as the zero flux state.

In the special case of XXZ quantum spin ice ($j_{z\pm} = j_{\pm\pm} = 0$), we see that the $\langle a\rangle$ and $\langle b\rangle$ sublattices are decoupled which means that the charge is separately conserved on both sublattices: $U(1)_{\text{all}} = U(1)_{\langle a\rangle} \otimes U(1)_{\langle b\rangle}$. It follows that we need only to solve the theory on one of the two sublattices, such that we are left with (choosing the $\langle a\rangle$ sublattice):

$$\mathscr{H}_{\text{s}}^0 = \sum_{\boldsymbol{x}\in\langle b\rangle}\frac{\hat{Q}_{\boldsymbol{x}}^2}{2} - \frac{j_{\pm}}{4}\sum_{\boldsymbol{x}\in\langle a\rangle}\sum_{\mu<\nu}\psi_{\boldsymbol{x}+\mu}^{\dagger}\psi_{\boldsymbol{x}+\nu} + H.c. \quad , \tag{3.3}$$

where $\psi_{\boldsymbol{x}+\mu}, \psi_{\boldsymbol{x}+\nu}$, with $\boldsymbol{x} \in \langle a\rangle$ live on the $\langle b\rangle$ sublattice.

In previous works, the rotor model (3.3) was solved by relaxing the local constraint $\psi_{\boldsymbol{x}}^{\dagger}\psi_{\boldsymbol{x}} = 1$ to a global constraint $\sum_{\boldsymbol{x}}\left(\psi_{\boldsymbol{x}}^{\dagger}\psi_{\boldsymbol{x}} - 1\right) = 0$. This can be regarded as a large-N approximation (see section 1.4.1) for an O(N) rotor. The XY rotor used here has $N = 1$.

3.1.1 "Exclusive" boson representation

Here we adopt an alternative approximation scheme by introducing a novel bosonic representation of a quantum XY rotor similar to the well-known Holstein-Primakoff boson representation of spins [75]:

$$\psi = \frac{1}{\sqrt{1 + d^{\dagger}d + b^{\dagger}b}}\left(d + b^{\dagger}\right), \tag{3.4}$$

$$\hat{Q} = d^{\dagger}d - b^{\dagger}b. \tag{3.5}$$

The d and b bosons carry positive and negative charge, respectively. To enforce the $\psi^{\dagger}\psi = 1$ constraint, we demand that the two species of bosons cannot appear simultaneously on the same site hence the name "exclusive" boson. Defining $n_b = b^{\dagger}b$ and $n_d = d^{\dagger}d$, the constraint translates into:

$$n_b n_d = 0, \tag{3.6}$$

which means that the constrained Hilbert space ($\mathscr{H}_{b,d}$) of the exclusive bosons is spanned by $\{|n_d, 0\rangle\} \otimes \{|0, n_b\rangle\}$, $n_d, n_b \in \mathbb{N}$, with the additional specification that we do not double count the $|0,0\rangle$ state. Recall that the dimension of the rotor Hilbert space is $2Q^{\max}+1$ where $Q^{\max}$ is the maximum charge allowed on each site. The exclusive boson representation shares the same Hilbert space (using $n_b^{\max} = n_d^{\max} = Q^{\max}$) such that the dimension of the exclusive boson Hilbert space is $dim(\mathscr{H}_{b,d}) = n_b^{\max} + n_d^{\max} + 1 = 2Q^{\max} + 1$. Finally, the representation Eq. (3.4) and Eq. (3.5) reproduces the desired commutation relations and properties of the rotors (see Eq. (2.3)):

$$\psi\psi^\dagger = \frac{1}{\sqrt{1 + d^\dagger d + b^\dagger b}} \left(dd^\dagger + b^\dagger b + db + b^\dagger d^\dagger\right) \frac{1}{\sqrt{1 + d^\dagger d + b^\dagger b}} \tag{3.7}$$

$$= \frac{1}{\sqrt{1 + d^\dagger d + b^\dagger b}} \left(dd^\dagger + b^\dagger b\right) \frac{1}{\sqrt{1 + d^\dagger d + b^\dagger b}} = 1, \tag{3.8}$$

where in the last line we used the canonical commutation relation for bosons: $[b, b^\dagger] = [d, d^\dagger] = 1$. Similarly, one can show that $[\psi, \hat{Q}] = \psi$. Thus, the exclusive bosons are a faithful representation of the $N = 1$ rotor.

3.1.2 Dilute boson limit

We rewrite the spinon Hamiltonian (3.3) using pairs of exclusive bosons defined separately on every site $\boldsymbol{x}$. We note that the exclusiveness applies only on-site:

$$n_{b,\boldsymbol{x}} n_{d,\boldsymbol{x}'} = n_{b,\boldsymbol{x}} n_{d,\boldsymbol{x}'} (1 - \delta_{\boldsymbol{x},\boldsymbol{x}'}). \tag{3.9}$$

We normal-order $\hat{Q}_{\boldsymbol{x}}^2$ with respect to the classical vacuum, or classical spin ice states (i.e without spinons):

$$\hat{Q}_{\boldsymbol{x}}^2 = d_{\boldsymbol{x}}^\dagger d_{\boldsymbol{x}} + b_{\boldsymbol{x}}^\dagger b_{\boldsymbol{x}} + d_{\boldsymbol{x}}^\dagger d_{\boldsymbol{x}}^\dagger d_{\boldsymbol{x}} d_{\boldsymbol{x}} + b_{\boldsymbol{x}}^\dagger b_{\boldsymbol{x}}^\dagger b_{\boldsymbol{x}} b_{\boldsymbol{x}}. \tag{3.10}$$

Assuming the boson densities are low for small $j_\pm$ in the quantum spin ice or $U(1)$ spin liquid, we neglect the interaction between the bosons as well as their exclusiveness. The validity of these approximation was verified using exact diagonalization using a 2-site rotor model. It reproduces the correct low-energy spectrum, i.e. it has the spectrum degeneracies and retains the correct evolution of the spectrum with respect to $j_\pm$ as long as $j_\pm$ is small. Further arguments which validates this mapping are made in subsequent sections. To keep the level of notation minimal, we use hereafter $\psi_{\boldsymbol{x}}$ to imply its lowest order bosonic approximation:

$$\psi_{\boldsymbol{x}} \approx d_{\boldsymbol{x}} + b_{\boldsymbol{x}}^\dagger, \tag{3.11}$$

where we have neglected the square root in Eq. (3.4) since it contains density terms. The original spinon Hamiltonian (3.3) then becomes:

$$\mathscr{H}_{\rm s}^0 \approx \frac{1}{2}\sum_{\boldsymbol{x}\in\langle b\rangle} b_{\boldsymbol{x}}^\dagger b_{\boldsymbol{x}} + d_{\boldsymbol{x}}^\dagger d_{\boldsymbol{x}} - \frac{j_\pm}{4}\sum_{\boldsymbol{x}\in\langle a\rangle}\sum_{\mu<\nu}(d_{\boldsymbol{x}+\mu}^\dagger + b_{\boldsymbol{x}+\mu})(d_{\boldsymbol{x}+\nu} + b_{\boldsymbol{x}+\nu}^\dagger) + H.c. \tag{3.12}$$

We write the bosons in terms of their Bloch modes:

$$b_{\boldsymbol{x}} = \frac{1}{\sqrt{V}}\sum_{\boldsymbol{k}} e^{i\boldsymbol{k}\cdot\boldsymbol{x}} b_{\boldsymbol{k}} \quad , \quad d_{\boldsymbol{x}} = \frac{1}{\sqrt{V}}\sum_{\boldsymbol{k}} e^{i\boldsymbol{k}\cdot\boldsymbol{x}} d_{\boldsymbol{k}}. \tag{3.13}$$

Thus:

$$\mathscr{H}_{\rm s}^0 = \frac{1}{2}\sum_{\boldsymbol{k}} b_{\boldsymbol{k}}^\dagger b_{\boldsymbol{k}} + d_{\boldsymbol{k}}^\dagger d_{\boldsymbol{k}} - \frac{j_\pm}{4}\sum_{\boldsymbol{k}} \rho_{\boldsymbol{k}}(d_{\boldsymbol{k}}^\dagger + b_{-\boldsymbol{k}})(d_{\boldsymbol{k}} + b_{-\boldsymbol{k}}^\dagger). \tag{3.14}$$

The dispersion for the quasiparticles is obtained by a Bogolyubov transformation (see Appendix C):

$$\mathscr{H}_{\rm s}^0 = \sum_{\boldsymbol{k}}\left[\left(\omega_{\boldsymbol{k}} - \frac{1}{2}\right) + \omega_{\boldsymbol{k}}\left(\tilde{d}_{\boldsymbol{k}}^\dagger \tilde{d}_{\boldsymbol{k}} + \tilde{b}_{-\boldsymbol{k}}^\dagger \tilde{b}_{-\boldsymbol{k}}\right)\right], \tag{3.15}$$

where the form of $\tilde{d}_{\boldsymbol{k}}$ and $\tilde{b}_{\boldsymbol{k}}$ are given in Appendix C and where:

$$\omega_{\boldsymbol{k}} = \frac{1}{2}\sqrt{1 - 2j_\pm\rho_{\boldsymbol{k}}}, \qquad \rho_{\boldsymbol{k}} = \sum_{\mu<\nu}\cos\left(\boldsymbol{k}\cdot(\mathbf{e}_\mu - \mathbf{e}_\nu)\right). \tag{3.16}$$

This single-spinon dispersion relation is plotted in Figure 3.1. The minimum of this dispersion relation is located at the $\boldsymbol{k} = (0,0,0)$ point (Γ point). The $j_\pm$ critical value at which the dispersion becomes gapless, thus leading to a condensation of the spinon, is simply given by $j_\pm^c = 1/12 \approx 0.083$. We see that this critical point is smaller than the value found by Savary *et al.* (see Fig. 2.1) of $j_\pm^c = 0.192$. In fact our approximation scheme provides a great improvement on the estimation of the critical point since quantum Monte Carlo studies of Ref. [53] found a critical value of $j_\pm^{QMC} \approx 0.05$.

Consistency checks We remark that in the classical limit ($j_\pm \to 0$), $\omega_{\boldsymbol{k}} \to 0.5$ agreeing with the expectations that a single spinon cost $J_{zz}/2$ in energy. The zero-point energy density of our exclusive boson Hamiltonian is given by:

$$E_0 = \frac{2}{V}\sum_{\boldsymbol{k}}\left(\omega_{\boldsymbol{k}} - \frac{1}{2}\right), \tag{3.17}$$

where the factor of 2 takes into account the fact that we have 2 copies of the same Hamiltonian (on the $\langle a \rangle$ and $\langle b \rangle$ diamond sublattices). For small $j_\pm$, the zero-point energy is:

$$E_0 = -\frac{3}{2} j_\pm^2 - 3 j_\pm^3 + \mathcal{O}(j_\pm^4), \tag{3.18}$$

such that for $j_\pm = 0$, we recover $E_0 = 0$ as expected for classical spin ice. Overall, we see that the exclusive boson representation is reliable. However, in this section we have only studied a regime where $|j_\pm|$ quite small. In fact, in the following section, we provide evidence that the dilute boson approximation is likely to break down for $|j_\pm| \gtrsim 0.2$ by computing self-consistently the boson density as a function for $j_\pm$.

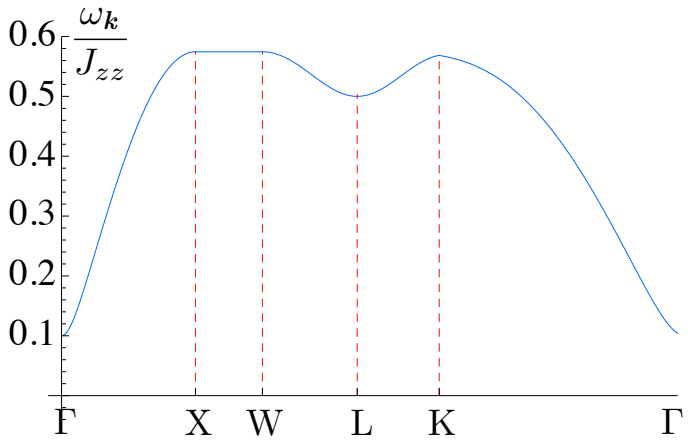

Figure 3.1: Single spinon dispersion (Eq. (3.16)) relation for the zero-flux state along the high symmetry directions of the FCC lattice for $j_\pm = 0.08$. See Appendix F.1 to visualize the high symmetry points.

3.2 Frustrated XXZ quantum spin ice ($j_\pm < 0$)

In the case where $j_\pm < 0$, the planar components of the spins of the original XXZ QSI Hamiltonian are frustrated. Recall that at the beginning of this Chapter we observed that the static part of the gauge-fields may be deduced from perturbative results. This is true since taking $U \sum_{\boldsymbol{x}} E^2_{\boldsymbol{x},\boldsymbol{x}\mu} = 0$ is precisely the limit were the gauge-fields are static. To lowest order in perturbation theory with $j_\pm < 0$, one finds that the preferred static gauge-field configuration is one for which the flux across each hexagonal plaquette is $B_{\hexagon} = \pi$

[4]. We will hereafter refer to this state as the π-flux state. However, one may inquire wether this is a correct choice for higher order terms obtained via perturbation theory. We expect that for $j_{\pm} < 0$, a competition between different terms in the perturbative expansion will arise as a consequence of the inherent frustration of the planar component. More explicitly, the higher order terms obtained in the perturbative for XXZ quantum spin ice will have terms of the form $\tilde{c}\cos(B_{\hexagon} + B_{\hexagon'})$, with $\tilde{c} > 0$ that will not favour a π flux state through all hexagonal plaquettes. In the following subsection we carry out the analysis of the fourth and fifth order perturbation terms and show that new flux states are favored by these terms. After determining the form of all possible translationally-invariant spin liquid states we repeat an analysis similar to that in section 3.1.

3.2.1 Perturbative results

Here we discuss briefly certain features of the degenerate perturbation scheme using the so-called effective Hamiltonian method [76] (we give a more thorough presentation in Appendix B). This method relies on the fact that there is no crossing in between states belonging to the excited state manifolds and states of the spin ice manifold. Then, all non-trivial terms generated via perturbation theory, with the $j_\pm$ term taken as a perturbation, will be multi-spin exchange terms forming closed loops with alternating S^+, S^- around the loops. Given a multi-spin exchange term around a closed loop C, the resulting term after the mapping to rotor variables will simply be of the form $\cos(B_C)$ (again, B_C is the flux through a particular plaquette defined by C). In determining the form of the perturbative expansion we are only interested in the explicit form for B_C[1]. In order to write down the effective Hamiltonian in terms of the fluxes we first define a positive direction for the fluxes. We thus arbitrarily choose the flux coming out the pyrochlore lattice unit cell as being positive. These are the $[-1,1,1],[1,-1,1],[-1,-1,-1],[1,1,-1]$ directions. The right-hand rule is then used to express the flux in terms of the gauge-fields. Then, using the definition for the flux given by Eq. (2.14) we write an effective Hamiltonian that we give here for further references:

$$\mathcal{H}_{\text{eff}} = c_1 j_\pm^3 \sum_p \cos B_p + c_2 j_\pm^4 \sum_p \cos B_p + c_3 j_\pm^4 \sum_{\langle p,p'\rangle} \cos\left(B_p + B_{p'}\right) + \tag{3.19}$$

$$c_4 j_\pm^5 \sum_p \cos B_p + c_5 j_\pm^5 \sum_{\langle p,p'\rangle} \cos\left(B_p + B_{p'}\right) + c_6 j_\pm^5 \sum_{\langle p,p''\rangle} \cos(B_p - B_{p''}) + \tag{3.20}$$

$$c_7 j_\pm^5 \sum_{\langle p,p'''\rangle} \cos\left(B_p + B_{p'''}\right). \tag{3.21}$$

Let us clarify the notation. The center of the hexagonal plaquettes, denoted by p, form a pyrochlore lattice. A site p on this pyrochlore lattice has a first (p'), second (p'') and third[2] nearest-neighbour (p'''). We should emphasize here that the term of order $j_\pm^3$ can only selects $B_p = 0$ or $B_p = \pi$ for every plaquette. Higher order terms, however, are likely to induce more complicated flux states. The selected flux state for $\mathcal{H}_{\text{eff}}$ may be found using a classical Monte Carlo simulation (since $\mathcal{H}_{\text{eff}}$ is analogous to a classical XY model). Instead of pursuing an exhaustive search here, we instead consider some symmetric flux states.

[1] Exactly determining the form of the constants is a tedious but straightforward exercise. See [70] for an example of how this done.

[2] There are 2 types of third n.n. on the pyrochlore lattice. Here we refer to p''' as the third n.n. across an hexagonal plaquette.

We remark that the B_p are not independent but must satisfy:

$$\sum_{p\in \text{u.c.}} B_p = 2n\pi \ \forall \text{ u.c.} \quad (n \in \mathbb{Z}) \tag{3.22}$$

where the sum is carried over the four hexagonal plaquettes of a unit cell. This follows simply from the fact the gauge-fields on the unit cell formed by the four hexagonal loops (see Fig. 2.2) are each shared by two plaquettes. When calculating the flux with the right-hand rule, the gauge-field cancel by pairs up to a factor of $2\pi n$. This condition holds for all unit cell and reflects the quantization of the magnetic charge. From the latter constraint we find four simple symmetry *ansatz* that are translationally invariant at the level of a u.c.:

$$B_p = 0, \pm\frac{\pi}{2}, \pi \ \forall p. \tag{3.23}$$

Denoting the four plaquettes of the unit cell by B_1, B_2, B_3, B_4, then the four flux *ansatz* are:

- the zero-flux : $(B_1, B_2, B_3, B_4) = (0, 0, 0, 0)$;
- the π-flux : $(B_1, B_2, B_3, B_4) = (\pi, \pi, \pi, \pi)$;
- the "spin ice" flux : $(B_1, B_2, B_3, B_4) = (\pi/2, \pi/2, -\pi/2, -\pi/2)$;
- the "monopole" flux : $(B_1, B_2, B_3, B_4) = (\pi/2, \pi/2, \pi/2, \pi/2)$.

The latter two *ansatz* break time-reversal symmetry and thus correspond to chiral spin-liquid states [77]. Indeed, under time-reversal (TR) symmetry $B_i \to -B_i$ and we see that the zero flux and π-flux state are even under TR while the spin ice and monopole flux states are odd. The "spin ice" flux corresponds to having two $\pi/2$ fluxes going "in" the u.c. and two $\pi/2$ fluxes going "out" the u.c. which shares a similar rule as the 2-in/2-out rule of spin ice discuss in Chapter 1 (here however, we only consider a translational invariant state). This spin ice flux corresponds to a uniform magnetic field along one of the [100] directions. The "monopole" flux corresponds to a state supporting an effective charge-1 monopole according to (3.23).

They are many static gauge-field configuration that satisfy a given B_p *ansatz*. In Table 3.1 we give a specific gauge-field configuration for each of the four *ansatz*.

U(1) liquid	$\boldsymbol{q}_0$	$\boldsymbol{q}_1$	$\boldsymbol{q}_2$	$\boldsymbol{q}_3$
0-flux	0	0	0	0
π-flux	0	$2\pi\hat{x}$	$2\pi\hat{x}$	0
Monopole flux	0	$-\pi(\hat{x}+\hat{z})$	$\pi(\hat{x}+\hat{z})$	0
Spin ice flux	0	$\pi\hat{y}$	$-\pi\hat{y}$	0

Table 3.1: Gauge-field *ansatz* for all the possible translational invariant (at the level of the pyrochlore lattice cubic unit-cell) spin-liquid states: $e^{i\bar{A}_{\boldsymbol{x},\boldsymbol{x}\mu}} = e^{i\boldsymbol{q}_\mu\cdot\boldsymbol{x}}$ with $\boldsymbol{x}\in\langle a\rangle, \boldsymbol{x}+\mu\in\langle b\rangle$. For $e^{i\bar{A}_{\boldsymbol{x},\boldsymbol{x}\mu}}$ with $\boldsymbol{x}\in\langle b\rangle, \boldsymbol{x}-\mu\in\langle a\rangle$, we have $e^{i\bar{A}_{\boldsymbol{x},\boldsymbol{x}\mu}} = e^{i\boldsymbol{q}_\mu\cdot(\boldsymbol{x}-\mu)}$.

3.2.2 π-flux state

The spinon Hamiltonian (3.1) in terms of translationally invariant (at the level of a u.c.) gauge-field configurations $e^{i\bar{A}_{\boldsymbol{x},\boldsymbol{x}\mu}} = e^{i\boldsymbol{q}_\mu\cdot\boldsymbol{x}}$ assumes the form:

$$\mathscr{H}_{\rm s}^{\boldsymbol{q}} \approx \frac{1}{2}\sum_{\boldsymbol{x}\in\langle b\rangle} b^\dagger_{\boldsymbol{x}} b_{\boldsymbol{x}} + d^\dagger_{\boldsymbol{x}} d_{\boldsymbol{x}} - \frac{j_\pm}{4}\sum_{\boldsymbol{x}\in\langle a\rangle}\sum_{\mu<\nu}\psi^\dagger_{\boldsymbol{x}+\mu}\psi_{\boldsymbol{x}+\nu}e^{i(\boldsymbol{q}_\nu-\boldsymbol{q}_\mu)\cdot\boldsymbol{x}} + H.c. \tag{3.24}$$

In the case of the π-flux, the unit cell is doubled and thus the dispersion relation for this state will display two branches. After a Fourier transform, the second term of $\mathscr{H}_{\rm s}^{\boldsymbol{q}}$ for the π-flux reads:

$$h_{j_\pm} = -\frac{j_\pm}{4}\sum_{\boldsymbol{k}}\vec{\psi}^\dagger_{\boldsymbol{k}}\cdot M_{\boldsymbol{k}}\cdot\vec{\psi}_{\boldsymbol{k}}, \tag{3.25}$$

with $\vec{\psi}^\dagger_{\boldsymbol{k}} = \left(\psi^\dagger_{\boldsymbol{k}}, \psi^\dagger_{\boldsymbol{k}+\boldsymbol{Q}}\right)$ and $\boldsymbol{Q} = 2\pi\hat{x}$. Note that the sum is carried over the first reduced Brillouin zone since the unit cell in real space is doubled. The kernel $M_{\boldsymbol{k}}$ is given in Appendix E for future references. We then diagonalize $M_{\boldsymbol{k}} = U_{\boldsymbol{k}}\Lambda_{\boldsymbol{k}}U^\dagger_{\boldsymbol{k}}$ and define $U^\dagger_{\boldsymbol{k}}\cdot\psi_{\boldsymbol{k}} = (\psi_{\boldsymbol{k},1}, \psi_{\boldsymbol{k},2})^{\mathbf{T}}$. Finally, substituting $\psi_{\boldsymbol{k},i} = b^\dagger_{-\boldsymbol{k},i} + d_{\boldsymbol{k},i}$, we obtain:

$$\mathscr{H}_{\rm s}^{\boldsymbol{q}} = \frac{1}{2}\sum_{\boldsymbol{k}}\sum_{i=1}^{2}\left[d^\dagger_{\boldsymbol{k},i}d_{\boldsymbol{k},i} + b^\dagger_{-\boldsymbol{k},i}b_{-\boldsymbol{k},i} - \frac{j_\pm}{2}\Lambda_{\boldsymbol{k},i}\left(d^\dagger_{\boldsymbol{k},i}d_{\boldsymbol{k},i} + d^\dagger_{\boldsymbol{k},i}b^\dagger_{-\boldsymbol{k},i} + b_{-\boldsymbol{k},i}d_{\boldsymbol{k},i} + b_{\boldsymbol{k},i}b^\dagger_{\boldsymbol{k},i}\right)\right]. \tag{3.26}$$

$\Lambda_{\boldsymbol{k},i}$ are the eigenvalues of $M_{\boldsymbol{k}}$. Identically to the case of the zero-flux, the quasi-particle spectrum of this quadratic Hamiltonian is obtained via a Bogolyubov transformation. The dispersion relation branches are given by:

$$\omega_{\boldsymbol{k},i} = \frac{1}{2}\sqrt{1 - j_\pm\Lambda_{\boldsymbol{k},i}}, \quad i = 1, 2. \tag{3.27}$$

The dispersion relation along the high symmetry directions is presented in Fig. 3.2.

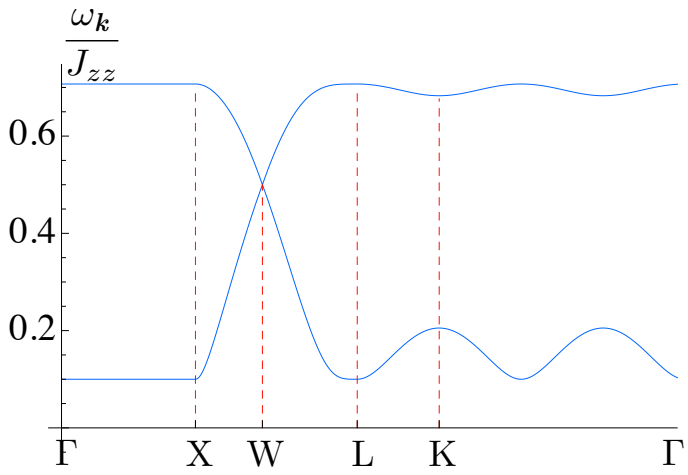

Figure 3.2: Single spinon dispersion relation for the π-flux state along the high symmetry directions of the FCC lattice for $j_{\pm} = -0.2$.

3.2.3 Spin ice and monopole flux states

The unit cell for the monopole and the spin ice flux state is quadrupled compared to unit cell of the zero-flux state and thus display four different branches. The dispersion relation is obtained via the same analytical procedure that we followed for the case of the π-flux state. We find:

$$\omega_{\boldsymbol{k},i} = \frac{1}{2}\sqrt{1 - j_{\pm}\Lambda_{\boldsymbol{k},i}}, \quad i = 1, 2, 3, 4. \tag{3.28}$$

The kernel of these flux states from which we deduce $\Lambda_{\boldsymbol{k},i}$ are given in Appendix E for future reference. The dispersions relation for these two states are presented in Figure 3.3.

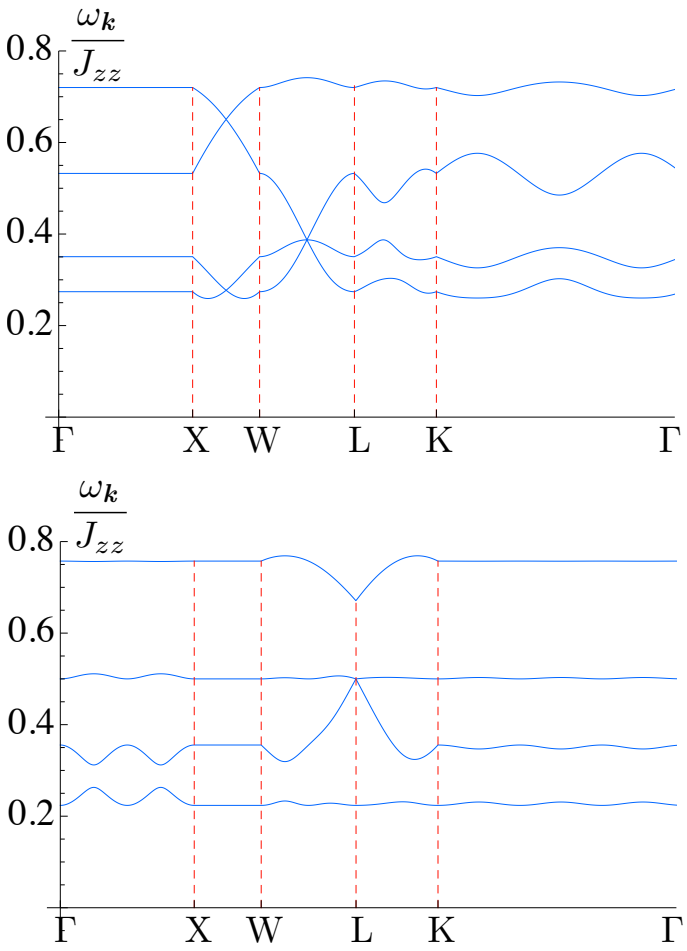

Figure 3.3: Single spinon dispersion relation for the monopole (top) and spin ice flux (bottom) states along the high symmetry directions of the FCC lattice for $j_{\pm} = -0.2$

3.2.4 Stability diagram for XXZ quantum spin-ice

The stability diagram for the $U(1)$ liquid obtained via the exclusive boson method is presented in Fig. 3.4. The boundaries indicated in the diagram correspond to the point where the spinon condenses.

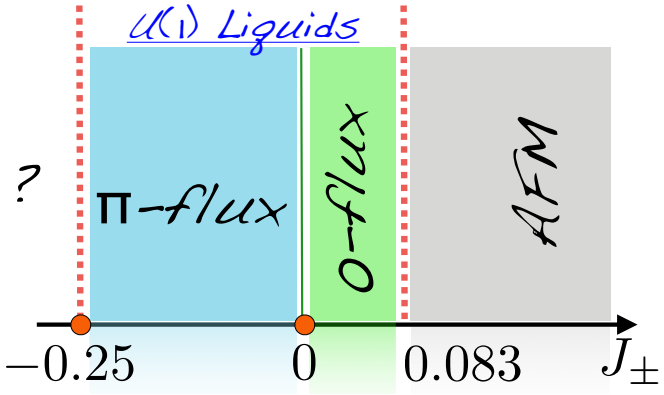

Figure 3.4: Stability diagram for the $U(1)$ liquids. The dotted line indicate the points at which the spinon condense while the green line indicates a first order like transition between the zero and the π-flux state. A question mark for $j_\pm < -0.25$ indicates that we have not pursued a rigorous analysis of the phase stabilized at $j_\pm < -0.25$. In fact, as we will see below, we expect that the dilute boson approximation breaks down in that regime. Note that $j_\pm = -1$ corresponds to the Heisenberg point.

3.2.5 Discussion

The dispersion relations for the π, the monopole and the spin ice flux present some very flat features. This effectively lowers the dimensionality of the system and is expected to stabilize the $U(1)$ liquid to larger values of $|j_\pm|$ than for the zero flux (where recall that we found a critical point of $j_\pm^c \approx 0.083$). In principle, the perfect flatness exhibited by the bands along some high-symmetry lines is not protected by any fundamental symmetry (i.e. it is "emergent")[4] and we expect that the addition of gauge-fluctuations or correlation effects will lift this degeneracy while preserving a certain degree of flatness. One may define the degree of flatness via the flatness ratio which is the band gap δ_b divided by the bandwidth t of a particular band [78]. The band gap is energy difference between the different branches of the dispersion relation. Unfortunately, in our analysis we find that

the band gap is vanishing for all flux states. This is clear for the π-flux and the monopole flux state in Fig. 3.3 and Fig. 3.2. The band crossing for the spin ice flux state occurs a point that is not along the high symmetry lines and thus is not seen in Fig. 3.3. It would be desirable to pursue a symmetry analysis of theses bands to try to identify possible ways to create a band gap (i.e. determine what type of perturbation, if any, can lift the degeneracies). Also, because the monopole and spin ice flux states break time-reversal symmetry, we expect that they might carry a non-trivial Chern number [39, 77]. The combination of the latter two features, i.e. a non-trivial Chern number and a large flatness ratio has been recently proposed as a promising way to realize the fractional quantum Hall effect without Landau levels [78].

3.2.6 Perspective from exact diagonalization

The dilute limit approximation for the exclusive boson representation is expected to fail for sufficiently large $|j_\pm|$. In Fig. 3.5, we have plotted the boson density $n \equiv \langle b^\dagger b + d^\dagger d \rangle$ for the selected flux state (zero-flux for $j_\pm > 0$ and π-flux for $j_\pm < 0$) as a function of $j_\pm$, using a self-consistent procedure that we detail in appendix 3.5. The boson density appears well controlled at the critical value $j_\pm = 1/12$ for the zero flux, with a density of $n \approx 0.03$, much smaller than the density in the high-temperature paramagnetic phase of spin-ice $n_{\text{para}} \approx (6 \times 0 + 8 \times 1 + 2 \times 2) = 0.75$. Thus we expect the dilute boson approximation to hold reasonably in that limit. Near the $j_\pm = -0.25$ point however, the density is about $n \approx 0.15$ which indicates that the boson correlations may play a non-trivial role.

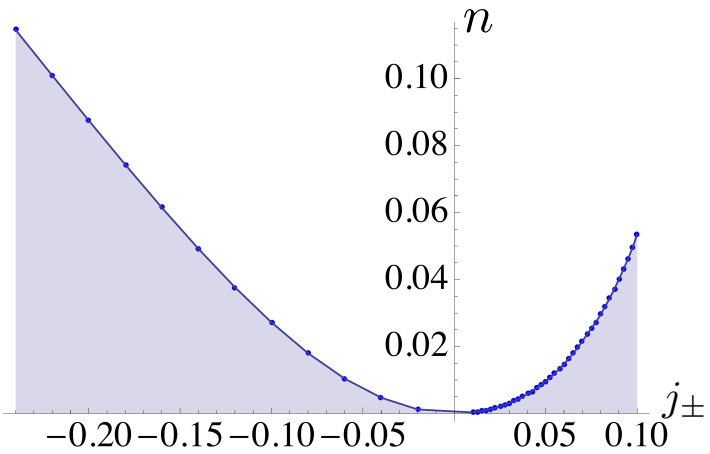

Figure 3.5: Boson density $n \equiv \langle b^\dagger b + d^\dagger d \rangle$ calculated within a self-consistent procedure in the exclusive boson formalism (see Appendix C for more details).

In order to investigate this possibility in a straightforward and simple manner, we have performed exact diagonalization of the rotor model Eq.(3.1) for two types of cluster. The choice of clusters for ED is based on the following requirements :

1. Preserve as many symmetries of the diamond lattice as possible (see Appendix 1.2);
2. Include as many loops as possible;

Based on these criteria, we studied two clusters with open boundary conditions (see Fig. 3.7 to visualize the clusters on the pyrochlore lattice). In the ED we truncate the Hilbert space at $|Q_{\boldsymbol{x}}| \leq 2$ which corresponds to the physical constraint of having at most 2 spinons per site. The cluster size are rather limited. The largest cluster one can treat fairly simply is a 10 site cluster[3]. Of course, since we are studying only two clusters, we do not attempt any finite size scaling [46] and focus only on the qualitative features.

The results are shown in Fig. 3.6. We see that the 4 sites cluster reproduces qualitatively the phase diagram obtained via the exclusive boson method. This was to be expected since a 4 site cluster only contains small hexagon loops is thus expected to incorporate only the physics of the zero or π flux states. This is in contrast with the 10 site cluster where in fact we found evidence that the spin-ice flux is selected at sufficiently negative $j_\pm$. The "condensation" of that state is observed after the point where the π-flux and spin ice flux cross in energy (see Fig. 3.9).

[3]Combining the $U(1)$ symmetry, a sparse matrix representation and some extreme eigenvalues algo-

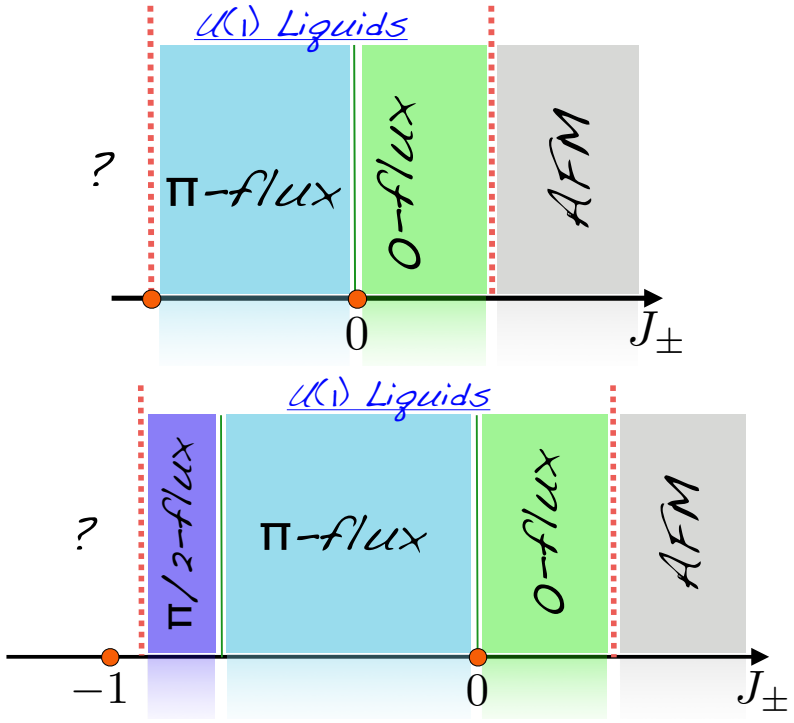

Figure 3.6: Stability diagram obtained via exact diagonalization. (top) The $N = 4$ cluster calculations. (bottom) The $N = 10$ cluster calculations. The dashed lines represent condensation and the green lines represent first-order phase transitions w/o condensation. The critical points along the $j_\pm$ axis are $j_\pm = -0.9$ for the spin ice flux condensation point, $j_\pm = -0.73$ for the π-flux to spin-ice flux transition, $j_\pm = 0$ for the π-flux to zero-flux transition and $j_\pm = 0.6$ for the zero-flux condensation.

Estimation of the critical points in exact diagonalization In ED, it is possible to estimate the quantum critical point at which the spinon condenses. Since we are only studying a finite size system the gap never closes but instead is expected to reach a minimum value in the vicinity of the critical point (see Fig. 3.8). The ED estimation (with the $N = 10$ cluster and charge-1 truncation) of the critical points along the $j_\pm$ axis are $j_\pm \approx -0.9$ for the spin-ice flux condensation point, $j_\pm \approx -0.73$ for the π-flux to spin-ice flux transition, $j_\pm = 0$ for the π-flux to zero-flux transition and $j_\pm \approx 0.6$ for the zero-flux condensation.

rithms.

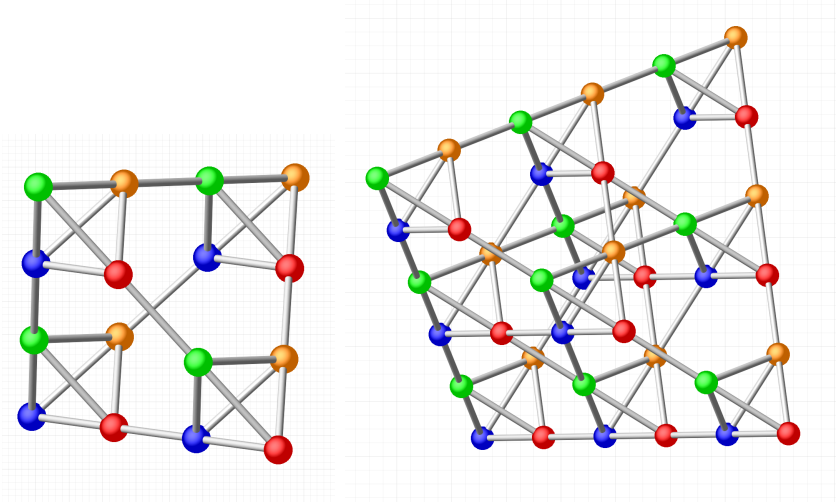

Figure 3.7: The 4 and 10 sites clusters studied (more precisely the dual version of these clusters). The coloring represents that 4 sublattices of the pyrochlore lattice. The 4 sites and 10 sites clusters are used to study the $j_{\pm}$ axis with $|Q_{\boldsymbol{x}}| \leq 2$ truncation.

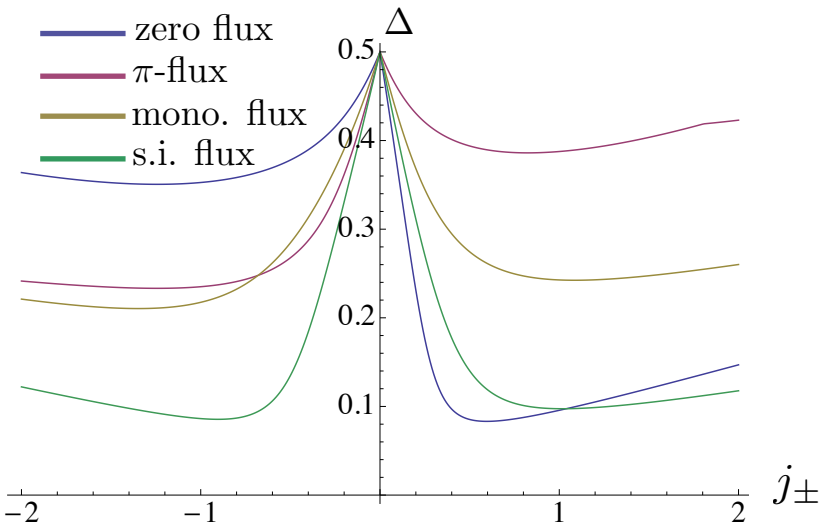

Figure 3.8: Gap (Δ) for the different flux states obtained from ED for the $N = 10$ cluster. The minima of the gap function are taken as an estimation of the condensation points for the thermodynamic (infinite) system.

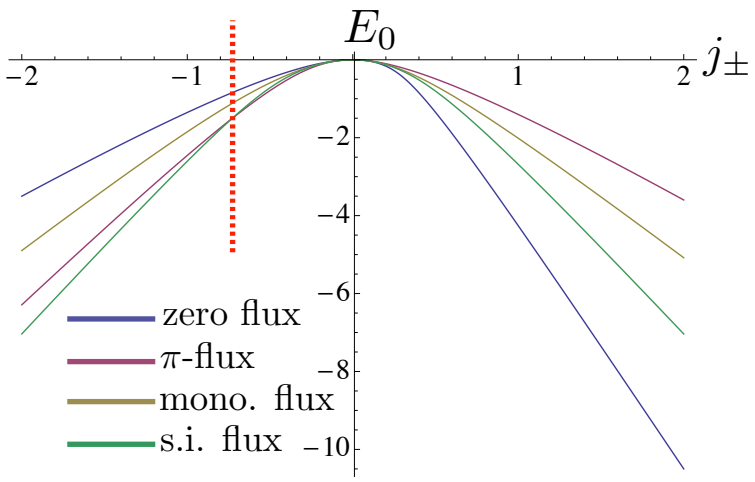

Figure 3.9: Ground-state energy for the different flux states obtained from ED for the $N = 10$ cluster. The doted red line indicates the crossing point between the spin ice flux state and the π flux state.

3.3 Summary

In summary, in this Chapter we have studied the matter sector of the $U(1)$ gauge theory that describes XXZ quantum spin ice. We have carried out a perturbative analysis of the XXZ quantum spin ice Hamiltonian and obtained a way to constrain the search for flux *ansatz* . Introducing a novel "exclusive" boson representation we have investigated the quantum rotor model that represents the matter sector of the gauge theory. The possibility of two novel chiral spin liquid that may (under suitable conditions) be promising states for supporting fractional quantum Hall physics, was envisioned. Finally, using exact diagonalization calculations, we have provided evidence that in fact one of chiral spin liquid state (the spin ice flux state) may be selected at sufficiently large $|j_{\pm}|$, with $j_{\pm} < 0$, when boson correlations become important.

Chapter 4

Conclusion

In this thesis, we have explored and described the low-energy physics of XXZ quantum spin ice. We began our analysis from a slave-rotor formulation of the XXZ quantum spin ice. This formalism was introduced by Savary *et al.*[3] in order to describe the predicted $U(1)$ quantum spin liquid phase of quantum spin ice. Using insights provided by degenerate perturbation theory, we have explored the possibility of realizing new spin liquids that break time-reversal symmetry. Such states are expected to have intriguing properties and may even support fractional quantum Hall states. Althought we haven't fully addressed such possibilities, we believe that this is an important motivation for future work. In performing this analysis, we believe we have established the basic formalism to characterize the matter sector of quantum spin-ice by introducing a novel "exclusive" boson representation of a XY quantum rotor. This novel representation for XY rotors is general and may be applied to other problems in which the interacting degrees of freedom are represented by rotors.

While in this work we have considered only the non-interacting limit (or dilute limit) of quantum spin ice, extension of our approach using the standard tools of many-body theory to treat correlation effects could be employed to carry out further investigations. Exact diagonalization calculations has provided evidence for the existence of a chiral spin liquid in the strong correlation regime (when $|j_{\pm}| \sim 1$), in the vicinity of the Heisenberg point. It is likely that the only reliable (yet still biased) method to explore that limit is variational Monte Carlo using trial wave-functions based on insights provided in analysis such as the one carried out in this thesis.

Quantum spin-ice is a very rich and challenging problem because few unbiased methods can be used to study three dimensional quantum frustrated magnets. Because of that, multiple theoretical work using different methods are required to understand the exotic

physics at play in these systems. We should also emphasize that quantum spin ice physics is a subject of rapidly mounting interest in the condensed matter community since to be realized in a number of rare-earth pyrochlore oxide compounds: it thus provides us with an almost unique possibility to study quantum spin liquid physics from both an experimental and theoretical point of view. The current work was focussed on studying the ground-state properties of quantum spin ice and its spinon excitations. Extension of the work to finite temperature is required in order to bridge the gap between theory and experiment [69, 70]. Also, the effect of the interaction between the gauge-fields and the spinons for XXZ remains an open problem. Finally, we should mention that while we have focussed our attention towards the XXZ quantum spin-ice limit, other anisotropic interactions are expected to play an important role in the physics of an experimentally realized quantum spin ice system.

APPENDICES

Appendix A

Pyrochlore Lattice

The pyrochlore lattice is a face-centered cubic (FCC) lattice with four sublattices. It is described by the $Fd\bar{3}m$ space group [56] and the cubic O_h point group. Some symmetry of pyrochlore lattice symmetries that are easy to visualize are the C_3 symmetry about the [111] cubic diagonals and the C_2, C_2' symmetries about the [110] and [100] directions. Finally, we note that the pyrochlore lattice has and inversion point i. The reader is referred to Ref. [79] for the full character table of the O_h point group. The unimodular matrix that appears in the general Hamiltonian for nearest-neighbor quantum spin ice is given by:

$$\gamma_{\mu\nu} = \begin{cases} 1 & \text{if } \mathbf{e}_\mu - \mathbf{e}_\nu \in yz \text{ plane} \\ e^{i2\pi/3} & \text{if } \mathbf{e}_\mu - \mathbf{e}_\nu \in yz \text{ plane} \\ e^{-i2\pi/3} & \text{if } \mathbf{e}_\mu - \mathbf{e}_\nu \in xy \text{ plane} \end{cases} \tag{A.1}$$

$\mathbf{e}_0$	$(\hat{x}+\hat{y}+\hat{z})/4$
$\mathbf{e}_1$	$(\hat{x}-\hat{y}-\hat{z})/4$
$\mathbf{e}_2$	$(-\hat{x}+\hat{y}-\hat{z})/4$
$\mathbf{e}_3$	$(-\hat{x}-\hat{y}+\hat{z})/4$

Table A.1: Pyrochlore lattice sublattice vectors represented in Fig. A.1.

	$\hat{x}_i$	$\hat{z}_i$
site $i = 0$	$(-2, 1, 1)/\sqrt{6}$	$(1, 1, 1)/\sqrt{3}$
site $i = 1$	$(-2, -1, -1)/\sqrt{6}$	$(1, -1, -1)/\sqrt{3}$
site $i = 2$	$(2, 1, -1)/\sqrt{6}$	$(-1, 1, -1)/\sqrt{3}$
site $i = 3$	$(2, -1, 1)/\sqrt{6}$	$(-1, -1, 1)/\sqrt{3}$

Table A.2: Local reference for each sublattice of the pyrochlore lattice as represented in Fig. A.1 with $\hat{y}_i = \hat{z}_i \times \hat{x}_i$

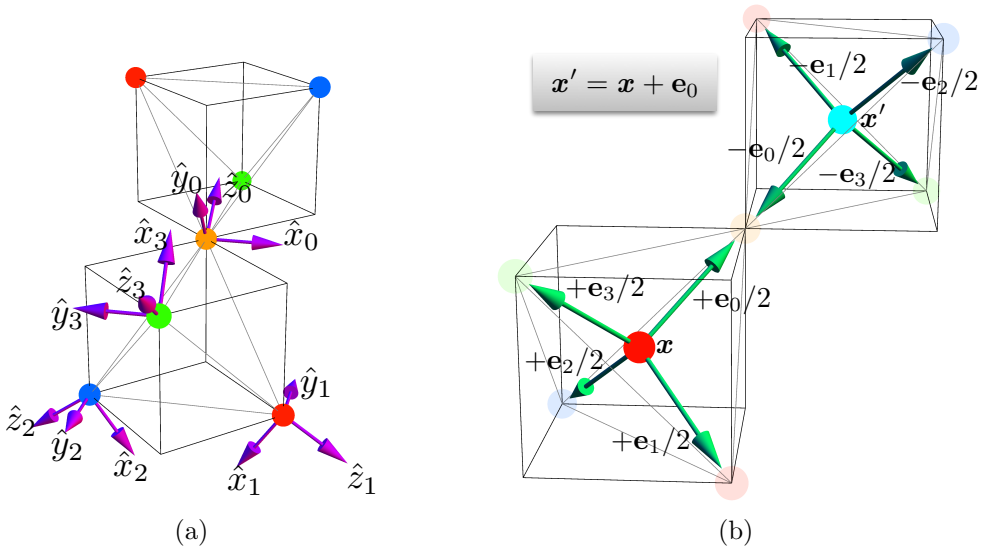

(a) (b)

Figure A.1: (a) Two inversion-related tetrahedra. On the lower tetrahedron the local reference frame of each sublattice (distinguished by the different sphere colors) is represented by the purple arrows. These local reference frames are given in Table A.2. (b) The diamond lattice is dual to the pyrochlore lattice. Here two sites (the red and cyan spheres) are represented. The diamond lattice is bipartite and we denote the lattice to which the red (cyan) sphere belongs as the A (B) sublattice. The pyrochlore lattice sites position are obtained from $\boldsymbol{x} + \mathbf{e}_\mu/2$ ($\mu = 0, 1, 2, 3$) with $\boldsymbol{x}$ on the diamond lattice. The $\mathbf{e}_\mu$ values are given in Table A.1.

Appendix B

Effective Hamiltonian Method

B.1 Foreword

Here we briefly review the effective Hamiltonian method [80, 76] obtained via standard Rayleigh-Schr'odinger perturbation theory. However, before we embark in this calculation, we would like emphasize two points that may be relevant for future work. First, the particular degenerate perturbation theory (DPT) scheme used should not influence the physics contained in the effective Hamiltonian obtained. Different (DPT) schemes generally lead to seemingly different effective Hamiltonians. However these effective Hamitonians, for a given order in perturbation theory, should be related by unitary transformation [81] and thus describe the same physics. Another relevant point to highlight is that the operators in the effective Hamiltonian method are not the same as those in the original theory. Thus the average $\langle S_i^x \rangle_{full}$ of the full theory (with respect to the full Hamiltonian) does not simply translate into $\langle S_i^x \rangle_{eff}$ (the average is taken w.r.t. to the effective Hamiltonian) in the effective theory. We refer the reader to Ref. [81] for further clarifications.

B.2 Degenerate perturbation theory

We consider an Hamiltonian of the form $H = H_0 + H_1$, where H_0 is easily solvable but H is not. We want to describe the effect of H_1 on the spectrum of H_0 for $H_1 \ll H_0$. Assume (as it is the case for the spin-ice Hamiltonian) that the spectrum of H_0 splits into distinct groups of closely-spaced levels such that energy separation between each state of the same group is much smaller than the energy difference between states of different groups.

We define:

$$\{|\psi_0^n\rangle\} \quad n = 1, \cdots, p, \tag{B.1}$$

as the p states that form the ground-state manifold of H. The ground-state manifold of H_0 is denoted: $\{|\varphi_0^n\rangle\}$ with $n = 1, \cdots, p$. Thus,

$$H_0 |\varphi_0^n\rangle = E_0 |\varphi_0^n\rangle , \tag{B.2}$$
$$H |\psi_0^n\rangle = \bar{E}_{0,n} |\psi_0^n\rangle . \tag{B.3}$$

We will refer to $\{|\varphi_0^n\rangle\}$ as the model space $\mathcal{M}$. The projector onto that model space is:

$$\mathcal{P} \equiv \sum_{n=1}^{p} |\varphi_0^n\rangle\langle\varphi_0^n| , \tag{B.4}$$

such that $\mathcal{P} |\psi_0^n\rangle \equiv |U_0^n\rangle \in \mathcal{M}$ $(n = 1, \cdots, p)$. In general, for $H_1 \ll H_0$, $\{|U_0^n\rangle\}$ will form a non-orthogonal basis of $\mathcal{M}$. There is always a linear transformation that exist between the basis of a vector space. We denote this transformation as T:

$$T |U_0^n\rangle = |\varphi_0^n\rangle \quad n = 1, \cdots, p \tag{B.5}$$

Finally, we define:

$$L \equiv \sum_{n=1}^{p} |\psi_0^n\rangle\langle\varphi_0^n| \tag{B.6}$$

and the so-called wave operator $\Omega = LT$ [80] and we see that:

$$\Omega |U_0^n\rangle = |\psi_0^n\rangle \tag{B.7}$$

More importantly, we have:

$$PH\Omega P |U_0^n\rangle = \bar{E}_0^n |U_0^n\rangle . \tag{B.8}$$

From the latter property we define the effective Hamiltonian as:

$$H_{\text{eff}} = PH\Omega P, \tag{B.9}$$

Here of course Ω depends on H_1. Thus because exact eigenvalues of H, $\left\{\bar{E}_{0,n}\right\}$, are determined by Ω, our goal will be to compute Ω. We have that:

$$\Omega P |\psi_0^n\rangle = |\psi_0^n\rangle , \tag{B.10}$$

such that within this subspace:

$$P\Omega P\left|\psi_0^n\right\rangle = P\left|\psi_0^n\right\rangle; \qquad \text{i.e.} \quad P\Omega P = P. \tag{B.11}$$

Now, consider the Schr$\acute{}$odinger equation:

$$\left(\bar{E}_0^n - H_0\right)\left|\psi_0^n\right\rangle = H_1\left|\psi_0^n\right\rangle \Rightarrow \left(\bar{E}_0^n - H_0\right)P\left|\psi_0^n\right\rangle = PH_1\left|\psi_0^n\right\rangle \tag{B.12}$$

$$= \left(\bar{E}_0^n - H_0\right)\left|U_0^n\right\rangle = PH_1\left|\psi_0^n\right\rangle \tag{B.13}$$

$$\Rightarrow \left(\bar{E}_0^n - H_0\right)P\left|\psi_0^n\right\rangle = PH_1\Omega P\left|\psi_0^n\right\rangle \tag{B.14}$$

$$\Rightarrow \left(\bar{E}_0^n - H_0\right)\Omega P\left|\psi_0^n\right\rangle = H_1\Omega P\left|\psi_0^n\right\rangle \tag{B.15}$$

Now multiplying Eq. (B.14) from the left by $-\Omega$ and adding it to Eq. (B.15), we obtain:

$$[\Omega, H_0]\,P = H_1\Omega P - \Omega P H_1 \Omega P \tag{B.16}$$

Consider an expansion of Ω in terms of the relevant energy scale for H_1:

$$\Omega = 1 + \Omega^{(1)} + \Omega^{(2)} + \cdots. \tag{B.17}$$

Introducing the resolvent operator $R \equiv (E_0 - H_0)^{-1}Q$, with $Q \equiv 1 - P$:

$$R = \sum_{|\psi_\alpha^n\rangle, \alpha\neq 0} \frac{|\psi_\alpha^n\rangle\langle\psi_\alpha^n|}{E_0 - E_\alpha}, \tag{B.18}$$

where $|\psi_\alpha^n\rangle$ with $\alpha \neq 0$ are the excited states of H_0. Finally, using $V \equiv H_1$, substituting Eq. (B.17) into Eq. (B.16), and solving, order by order, we finally obtain a recursive formula for $\Omega^{(N)}$:

$$\Omega^{(N)}P = (E_0 - H_0)^{-1}\left[V\Omega^{N-1}P - \sum_{\alpha+\beta=N-1}\Omega^{(\alpha)}PV\Omega^{(\beta)}P\right]. \tag{B.19}$$

B.3 Effective Hamiltonian for XXZ quantum spin-ice

In the straightforward degenerate perturbation theory computation for (1.17) we find seven non-constant term when carrying the calculation up to order $J_\pm^5$:

$$\begin{aligned} H_{\text{eff}}^{\text{XXZ}} &= PVR_V^2P + PVR_V^3P + PVR_V^4P \\ &+ PVRR_VPVR_VP + PVR_VRR_VPVR_VP \\ &+ PVRR_V^2PVR_VP + PVRR_VPVR_V^2P + \mathcal{O}(V^6), \end{aligned} \tag{B.20}$$

where we have defined $R_V \equiv RV$. The different terms in this expansion can be represented using graph. Then it becomes a simple geometric exercise to find the different ways these diagrams can be embedded on the lattice in order to obtain Eq. (3.21).

B.3.1 How the operators transform

If one is interested in computing observables from the original theory, then additional care must be made. In fact, operators from the original theory must be transformed within the scheme of the effective Hamiltonian method. To see this, consider the following: we want to compute the expectation value of the operator A within the manifold that we are studying:

$$\langle \psi_0^n | \, A \, | \psi_0^n \rangle = \langle U_0^n | \, P \Omega^\dagger A \Omega P \, | U_0^n \rangle \, . \tag{B.21}$$

Thus we see that the operators transform as:

$$A \to P \Omega^\dagger A \Omega P, \tag{B.22}$$

where the wave operator Ω is determined by Eq. (B.19).

Appendix C

Further details about the "exclusive" bosons

C.1 Boson density

In the exclusive boson formalism, a simple way to study the effect of the increase of the boson density away from the $j_\pm = 0$ limit is to introduce a chemical potential: $\mu = n + 1/2$, with $n \equiv \langle b^\dagger b + d^\dagger d \rangle$ such that:

$$\hat{Q}^2_{\boldsymbol{x}} \approx \mu \left(d^\dagger_{\boldsymbol{x}} d_{\boldsymbol{x}} + b^\dagger_{\boldsymbol{x}} b_{\boldsymbol{x}} \right). \tag{C.1}$$

We can use:

$$\psi^\dagger_{\boldsymbol{x}} \approx \frac{d^\dagger_{\boldsymbol{x}} + b_{\boldsymbol{x}}}{\sqrt{1+2n}}. \tag{C.2}$$

One can then proceed as in section 3.1.2 to diagonalize the spinon Hamiltonian. The boson density is then found by solving the self-consistent equation $n = \langle b^\dagger b + d^\dagger d \rangle$.

C.2 Bogolyubov transformation

The Bogolyubov transformation used in Eq. (3.14) is given by:

$$d_{\boldsymbol{k}} = \cosh\theta_{\boldsymbol{k}} \tilde{d}_{\boldsymbol{k}} + \sinh\theta_{\boldsymbol{k}} \tilde{b}^\dagger_{-\boldsymbol{k}} \tag{C.3}$$

$$b_{\boldsymbol{k}} = \cosh\theta_{\boldsymbol{k}} \tilde{b}_{\boldsymbol{k}} + \sinh\theta_{\boldsymbol{k}} \tilde{d}^\dagger_{-\boldsymbol{k}} \tag{C.4}$$

where $\theta_{\boldsymbol{k}}$ is determined by asking for the coefficient of off-diagonal terms such as $\tilde{d}_{\boldsymbol{k}}\tilde{b}_{-\boldsymbol{k}}$ to finish. We find:

$$\tanh(2\theta_{\boldsymbol{k}}) = \frac{1}{2}\left(1 - \frac{1}{\rho_{\boldsymbol{k}}}\right), \tag{C.5}$$

in the case of the zero flux.

Appendix D

Large-N approximation for the quantum XY rotors

In this section we use the approximation introduced by Savary *et al.* [3] to solve the rotor model $\mathscr{H}_{\text{s}}(\hat{Q}_{\boldsymbol{x}}, \psi_{\boldsymbol{x}})$ given in Eq. 3.1. This section serves to clarify the similarities and differences between the "exclusive" boson method and the large-N approximation. We are also interested in verifying wether the monopole flux or spin ice flux state may be selected within their formalism.

In order to solve the quantum rotor model, Savary *et al.* used a representation for which the real and imaginary part of the rotor are mapped to position operators:

$$\psi_{\boldsymbol{x}} = \hat{x}_{\boldsymbol{x}} + i\hat{y}_{\boldsymbol{x}}. \tag{D.1}$$

This mapping is exact as long as $x_{\boldsymbol{x}}^2 + y_{\boldsymbol{x}}^2 = 1$. In order to take into account this constraint, they implemented the constraint in a large-N fashion, by introducing a single Lagrange multiplier that is tuned so that $\langle \hat{x}_{\boldsymbol{x}} + \hat{y}_{\boldsymbol{x}} \rangle = 1$ for every rotor on the lattice. Using this approximation, the Hamiltonian for the spinons in terms of Block modes reads:

$$H = \sum_{\boldsymbol{k}} \sum_{i,j} \frac{1}{2} \Pi_{i\boldsymbol{k}}^{\dagger} \Pi_{j\boldsymbol{k}} \delta_{ij} - \frac{j_{\pm}}{4} \psi_{i\boldsymbol{k}}^{\dagger} \tilde{M}_{ij}(\lambda, \boldsymbol{k}) \psi_{j\boldsymbol{k}} - 2\lambda. \tag{D.2}$$

Where $\tilde{M} = \lambda\delta_{ij} + (M_{\boldsymbol{k}})_{ij}$ and where $M_{\boldsymbol{k}}$ is the kernel used in the exclusive boson calculation and is given in appendix E. We have defined $\Pi_{i\boldsymbol{k}}^{\dagger}$ as the conjugate variable of $\psi_{\boldsymbol{x}}$, i.e. $\Pi_{i\boldsymbol{x}}^{\dagger} = \hat{p}_{\boldsymbol{x}}^{x} + i\hat{p}_{\boldsymbol{x}}^{y}$ with $[x_{\boldsymbol{x}}, p_{\boldsymbol{x}'}^{x}] = i\delta_{\boldsymbol{x},\boldsymbol{x}'}$ such that $[\psi_{\boldsymbol{x}}^{\dagger}, \Pi_{\boldsymbol{x}}] = 2i$. As before, we diagonalize

the kernel to obtain:

$$H = \sum_{\boldsymbol{k}} \sum_{i} \frac{1}{2} \tilde{\Pi}^{\dagger}_{i\boldsymbol{k}} \tilde{\Pi}_{i\boldsymbol{k}} - \frac{j_{\pm}}{4} \Lambda_{\boldsymbol{k},i} \tilde{\psi}^{\dagger}_{i\boldsymbol{k}} \tilde{\psi}_{i\boldsymbol{k}} - 2\lambda. \tag{D.3}$$

Where we have $\tilde{M} = U\Lambda U^{\dagger}$ and $\tilde{\Pi} = U^{\dagger}\Pi$ and $\tilde{\psi} = U^{\dagger}\psi$. The latter expression is just a collection of non-interacting harmonic oscillators since: $\tilde{\Pi}_{i\boldsymbol{k}} = \hat{p}^{x}_{i\boldsymbol{k}} + i\hat{p}^{y}_{i\boldsymbol{k}}$ and $\tilde{\psi}_{i\boldsymbol{k}} = \hat{x}_{i\boldsymbol{k}} + i\hat{y}_{i\boldsymbol{k}}$ such that:

$$H = \sum_{\boldsymbol{k}} \sum_{i} \frac{1}{2} \left(\hat{p}^{x}_{i\boldsymbol{k}} \hat{p}^{x}_{i,-\boldsymbol{k}} + \hat{p}^{y}_{i\boldsymbol{k}} \hat{p}^{y}_{i,-\boldsymbol{k}} \right) - \frac{j_{\pm}}{4} \Lambda_{\boldsymbol{k},i} \left(\hat{x}_{i\boldsymbol{k}} \hat{x}_{i,-\boldsymbol{k}} + \hat{y}_{i\boldsymbol{k}} \hat{y}_{i,-\boldsymbol{k}} \right) - 2\lambda. \tag{D.4}$$

Finally using:

$$a_{i,\boldsymbol{k}} = \sqrt{\frac{\omega_{\boldsymbol{k}_i}}{2}} \left(\hat{x}_{i,\boldsymbol{k}} + \frac{i}{\omega_{\boldsymbol{k}}} \hat{p}^{x}_{i,-\boldsymbol{k}} \right), \tag{D.5}$$

$$b_{i,\boldsymbol{k}} = \sqrt{\frac{\omega_{\boldsymbol{k}_i}}{2}} \left(\hat{y}_{i,\boldsymbol{k}} + \frac{i}{\omega_{\boldsymbol{k}}} \hat{p}^{y}_{i,-\boldsymbol{k}} \right), \tag{D.6}$$

we arrive at:

$$H = \sum_{\boldsymbol{k}} \sum_{i} \omega_{\boldsymbol{k},i} \left(a^{\dagger}_{i,\boldsymbol{k}} a_{i,\boldsymbol{k}} + b^{\dagger}_{i,\boldsymbol{k}} b_{i,\boldsymbol{k}} + 1 \right), \tag{D.7}$$

with $\omega_{\boldsymbol{k},i} = \sqrt{-j_{\pm}\Lambda_{\boldsymbol{k},i}/2}$. The zero-point energy is thus given by:

$$E_0 = \frac{2}{V} \sum_{\boldsymbol{k}} \sum_{i} \left(\omega_{\boldsymbol{k},i} - \lambda \right). \tag{D.8}$$

Assuming a ground-state with uncondensed spinon $|0\rangle$, the constraint $\langle \hat{x}^2_{\boldsymbol{x}} + \hat{y}^2_{\boldsymbol{x}} \rangle = 1$ to finding λ such that:

$$\frac{1}{2V} \sum_{i} \sum_{\boldsymbol{k}} \frac{U_{1i} U^{\dagger}_{i1}}{\omega_{i,\boldsymbol{k}}} = 1 \tag{D.9}$$

Discussion The stability diagram obtained from this approach is presented in Fig. D.1 and is identical to the stability diagram obtained by Ref.[3, 4]. Notice that the spinon for the π flux condenses at $j_{\pm} \approx -4.1$, which is much outside the regime of validity of the formalism use here. We also remark that in the limit where $j_{\pm} \to 0$, we find $\lambda \to 1/2$

such that $E_0 \to 1/2$. In the same limit $\omega_{\boldsymbol{k},i} \to 1$. These two limits do no agree with the expectations for classical spin-ice where the ground-state energy is zero and the cost for creating a single spinon is 1/2. Finally, we add that within this formalism, althought the spin-ice flux is never selected as a ground-state, it also never condenses. According to our calculations (within the formalism of the present section), the spin-ice is stable all the way down to $j_\pm \to -\infty$.

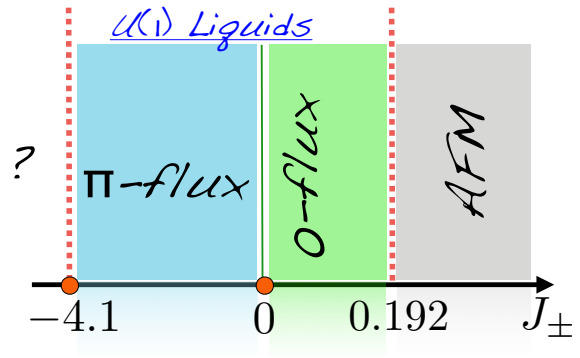

Figure D.1: Phase diagram for XXZ quantum spin ice obtained via the large-N approximation introduced by Ref. [3].

Appendix E

Kernel for computing the single spinon dispersion

When performing transforming the rotor operators to Block modes, one obtains a relation of the form:

$$\sum_{\boldsymbol{k}} \sum_{\mu,\nu} f_{\boldsymbol{k},\mu\nu} \psi^{\dagger}_{\boldsymbol{k}} \psi_{\boldsymbol{k}+g_{\mu\nu}} \equiv \sum_{\boldsymbol{k}} F(\boldsymbol{k}), \tag{E.1}$$

where $f_{\boldsymbol{k},\mu,\nu}$ is some function of $\boldsymbol{k}, \mu$ and ν. The $g_{\mu\nu}$ term is an integer multiple of $\boldsymbol{Q}$ where $\boldsymbol{Q} = (0,0,0)$ for the zero flux, $\boldsymbol{Q} = (2\pi,0,0)$ for the π-flux state, $\boldsymbol{Q} = (\pi,0,\pi)$ for the monopole flux state and $\boldsymbol{Q} = (0,\pi,0)$ for the spin ice flux state. Then writing Eq. (E.1) as a sum over the reduced Brillouin zone, we define the kernel $M_{\boldsymbol{k}}$ of the spinons. For instance, for the monopole flux with $\boldsymbol{Q} = (0,\pi,0)$ we have:

$$\sum_{\boldsymbol{k}} F(\boldsymbol{k}) = \sum_{\boldsymbol{k}\in BZ'} F(\boldsymbol{k}) + F(\boldsymbol{k}+\boldsymbol{Q}) + F(\boldsymbol{k}+2\boldsymbol{Q}) + F(\boldsymbol{k}+3\boldsymbol{Q}) \equiv \sum_{\boldsymbol{k}\in BZ'} \vec{\psi}^{\dagger}_{\boldsymbol{k}} \cdot M_{\boldsymbol{k}} \cdot \vec{\psi}_{\boldsymbol{k}} \tag{E.2}$$

with $\vec{\psi}_{\boldsymbol{k}} = (\psi_{\boldsymbol{k}}, \psi_{\boldsymbol{k}+\boldsymbol{Q}}, \psi_{\boldsymbol{k}+2\boldsymbol{Q}}, \psi_{\boldsymbol{k}+3\boldsymbol{Q}})^{\mathbf{T}}$

Kernel for the π flux We find (with $\boldsymbol{k} = k_x\hat{x} + k_y\hat{y} + k_z\hat{z}$):

$$(M_{\boldsymbol{k}})_{00} = -(M_{\boldsymbol{k}})_{11} = 2\cos\left(\frac{k_x}{2}\right)\cos\left(\frac{k_y}{2}\right), \tag{E.3}$$

$$(M_{\boldsymbol{k}})_{10} = -2\cos\left(\frac{k_z}{2}\right)\sin\left(\frac{k_y}{2}\right) + 2i\sin\left(\frac{k_x}{2}\right)\sin\left(\frac{k_z}{2}\right) \tag{E.4}$$

E.1 Kernel for the monopole flux

We find[1]:

$$(M_{\boldsymbol{k}})_{00} = -(M_{\boldsymbol{k}})_{22} = 2\cos\left(\frac{k_x + k_y}{2}\right) \tag{E.5}$$

$$(M_{\boldsymbol{k}})_{01} = e^{-\frac{1}{2}i(k_y+k_z)}\left(ie^{\frac{1}{2}i(k_x+k_y+2k_z)} + e^{\frac{1}{2}i(k_x+k_y)} + e^{ik_z} + 1\right) \tag{E.6}$$

$$(M_{\boldsymbol{k}})_{02} = 2i\sin\left(\frac{k_x - k_y}{2}\right) \tag{E.7}$$

$$(M_{\boldsymbol{k}})_{03} = e^{-\frac{1}{2}i(k_x+k_z)}\left(-i\left(-1 + e^{ik_z}\right)e^{\frac{1}{2}i(k_x+k_y)} + e^{ik_z} + i\right) \tag{E.8}$$

$$(M_{\boldsymbol{k}})_{11} = -(M_{\boldsymbol{k}})_{33} = -2\sin\left(\frac{k_x + k_y}{2}\right) \tag{E.9}$$

$$(M_{\boldsymbol{k}})_{12} = e^{-\frac{1}{2}i(k_x+k_z)}\left(-ie^{ik_z}\left(-1 + e^{\frac{1}{2}i(k_x+k_y)}\right) + e^{\frac{1}{2}i(k_x+k_y)} - i\right) \tag{E.10}$$

$$(M_{\boldsymbol{k}})_{13} = 2i\cos\left(\frac{k_x - k_y}{2}\right) \tag{E.11}$$

$$(M_{\boldsymbol{k}})_{23} = e^{-\frac{1}{2}i(k_y+k_z)}\left(ie^{ik_z}\left(e^{\frac{1}{2}i(k_x+k_y)} + i\right) + e^{\frac{1}{2}i(k_x+k_y)} - 1\right) \tag{E.12}$$

[1]Note that the kernel is different for the $\langle a\rangle$ and $\langle b\rangle$ sublattices. Here we give the kernel for the $\langle b\rangle$ sublattice.

E.2 Kernel for the spin ice flux

$$(M_{\boldsymbol{k}})_{00} = -(M_{\boldsymbol{k}})_{22} = 2\cos\left(\frac{k_x + k_y}{2}\right) \tag{E.13}$$

$$(M_{\boldsymbol{k}})_{01} = \sqrt[4]{-1}e^{-\frac{1}{2}i(k_x+k_z)}\left(\left(1+e^{ik_z}\right)e^{\frac{1}{2}i(k_x+k_y)} + \sin(k_z) - i\cos(k_z) + 1\right) \tag{E.14}$$

$$(M_{\boldsymbol{k}})_{02} = 2i\cos\left(\frac{k_x - k_y}{2}\right) \tag{E.15}$$

$$(M_{\boldsymbol{k}})_{03} = \sqrt[4]{-1}e^{-\frac{1}{2}i(k_y+k_z)}\left(-ie^{\frac{1}{2}i(k_x+k_y+2k_z)} + e^{\frac{1}{2}i(k_x+k_y)} + e^{ik_z} + 1\right) \tag{E.16}$$

$$(M_{\boldsymbol{k}})_{11} = -(M_{\boldsymbol{k}})_{33} = -2\sin\left(\frac{k_x + k_y}{2}\right) \tag{E.17}$$

$$(M_{\boldsymbol{k}})_{12} = \sqrt[4]{-1}e^{-\frac{1}{2}i(k_x+k_z)}\left(i\left(1+e^{ik_z}\right)e^{\frac{1}{2}i(k_x+k_y)} + \sin(k_z) - i\cos(k_z) + 1\right) \tag{E.18}$$

$$(M_{\boldsymbol{k}})_{13} = 2i\sin\left(\frac{k_x - k_y}{2}\right) \tag{E.19}$$

$$(M_{\boldsymbol{k}})_{23} = -\sqrt[4]{-1}e^{-\frac{1}{2}i(k_x+k_z)}\left(e^{ik_z}\left(e^{\frac{1}{2}i(k_x+k_y)} + i\right) + e^{\frac{1}{2}i(k_x+k_y)} - 1\right) \tag{E.20}$$

Appendix F

FCC Brillouin zone

F.1 First Brillouin zone of the FCC lattice

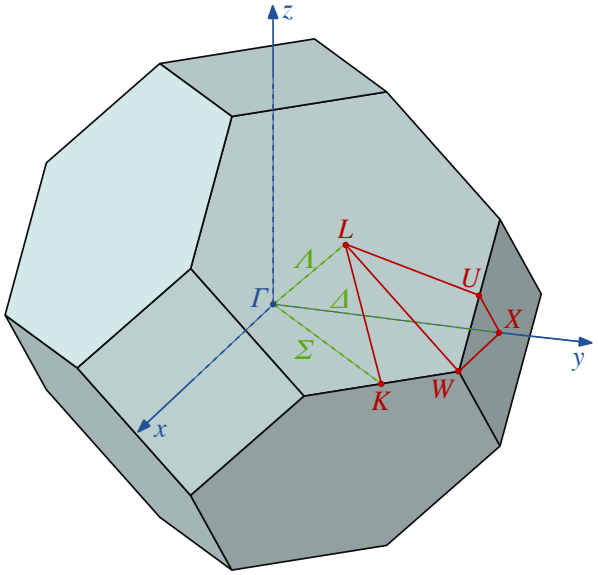

Figure F.1: Brillouin zone of the face cubic centered (FCC) lattice along with its high symmetry points.

F.2 Brillouin zone summation

The first Brillouin zone of a FCC lattice has the same shape of a truncated octahedron and is equivalent to the Wigner-Seitz cell of a BCC lattice [82]. For simplicity we carry out the Brillouin summations by summing over twice the FCC BZ and dividing the result by 2. Twice of the FCC BZ corresponds to a cube of volume $64\pi^3$ (we use $a = 1$ for the linear size of the conventional cubic cell of the pyrochlore lattice). Then, we have simply:

$$\sum_{\boldsymbol{k}} \to \frac{V}{64\pi^3} \int_{-2\pi}^{2\pi} \int_{-2\pi}^{2\pi} \int_{-2\pi}^{2\pi} \mathrm{d}k_x \mathrm{d}k_y \mathrm{d}k_z \tag{F.1}$$

As usual the summation is replaced by an integration, which is a valid manipulation as long as the summand does not diverge. A divergent summand requires additional care and we refer the reader to Ref. [3] for more details.

Bibliography

[1] M. J. Harris, S. T. Bramwell, D. F. McMorrow, T. Zeiske, and K. W. Godfrey. Geometrical frustration in the ferromagnetic pyrochlore $Ho_2Ti_2O_7$. *Phys. Rev. Lett.*, 79:2554–2557, Sep 1997.

[2] M. Hermele, M. P. A. Fisher, and L. Balents. Pyrochlore photons: The $u(1)$ spin liquid in a $s = 1/2$ three-dimensional frustrated magnet. *Phys. Rev. B*, 69:064404, Feb 2004.

[3] L. Savary and L. Balents. Coulombic quantum liquids in spin-1/2 pyrochlores. *Phys. Rev. Lett.*, 108:037202, Jan 2012.

[4] S. Lee, S. Onoda, and L. Balents. Generic quantum spin ice. *Phys. Rev. B*, 86:104412, Sep 2012.

[5] S. T. Bramwell and M. J. P. Gingras. Spin ice state in frustrated magnetic pyrochlore materials. *Science*, 294(5546):1495–1501, Nov 2001.

[6] R. Moessner and A. P. Ramirez. Geometrical frustration. *Phys. Today*, 59(2):24, Feb 2006.

[7] J.-F. Sadoc and R. Mosseri. Geometrical frustration. *Cambridge University Press*, Oct 1999.

[8] A.P. Ramirez. Geometrical frustration. *Handbook of magnetic materials*, 13:423–520, 2001.

[9] J. Villain. Insulating spin glasses. *Zeitschrift für Physik B Condensed Matter*, 33(1):31–42, Sep 1979.

[10] D.L. Bergman, J. Alicea, E. Gull, S. Trebst, and L. Balents. Order-by-disorder and spiral spin-liquid in frustrated diamond-lattice antiferromagnets. *Nature Physics*, 3(7):487–491, Jul 2007.

[11] J.D. Bernal and R.H. Fowler. A theory of water and ionic solution, with particular reference to hydrogen and hydroxyl ions. *Journal of Chemical Physics*, 1(8):515–548, Aug 1933.

[12] S. V. Isakov, K. Gregor, R. Moessner, and S. L. Sondhi. Dipolar spin correlations in classical pyrochlore magnets. *Phys. Rev. Lett.*, 93:167204, Oct 2004.

[13] L. Balents. Spin liquids in frustrated magnets. *Nature*, 464(7286):199–208, Mar 2010.

[14] L. Pauling. The structure and entropy of ice and of other crystals with some randomness of atomic arrangement. *J. Am. Chem. Soc.*, 57(12):pp 2680–2684, Dec 1935.

[15] D. Pomaranski, L.R. Yaraskavitch, S. Meng, K.A. Ross, H.M.L. Noad, H.A. Dabkowska, B.D. Gaulin, and J.B. Kycia. Absence of pauling's residual entropy in thermally equilibrated $Dy_2Ti_2O_7$. *Nature Physics*, Apr 2013.

[16] R.G. Melko, B.C. den Hertog, and M.J.P. Gingras. Long-range order at low temperatures in dipolar spin ice. *Phys. Rev. Lett.*, 87(6):067203, Jul 2001.

[17] R. Higashinaka, H. Fukazawa, D. Yanagishima, and Y. Maeno. Specific heat of $Dy_2Ti_2O_7$ in magnetic fields: comparison between single-crystalline and polycrystalline data. *Journal of Physics and Chemistry of Solids*, 63(6):1043–1046, Aug 2002.

[18] R. Siddharthan, B.S. Shastry, A.P. Ramirez, and A. Hayashi. Ising pyrochlore magnets: low-temperature properties,"ice rules," and beyond. *Phys. Rev. Lett.*, 83(9):1854–1857, Aug 1999.

[19] B. Klemke, M. Meissner, P. Strehlow, K. Kiefer, S.A. Grigera, and D.A. Tennant. Thermal relaxation and heat transport in the spin ice material $Dy_2Ti_2O_7$. *Journal of Low Temperature Physics*, 163(5-6):345–369, Feb 2011.

[20] C. Castelnovo, R. Moessner, and S. L. Sondhi. Magnetic monopoles in spin ice. *Nature*, 451(7174):42–45, Jan 2008.

[21] T. Fennell, P.P. Deen, A.R. Wildes, K. Schmalzl, D. Prabhakaran, A.T. Boothroyd, R.J. Aldus, D.F. McMorrow, and S.T. Bramwell. Magnetic coulomb phase in the spin ice $Ho_2Ti_2O_7$. *Science*, 326(5951):415–417, Sep 2009.

[22] J.B. Kogut. An introduction to lattice gauge theory and spin systems. *Reviews of Modern Physics*, 51(4):659, Oct 1979.

[23] O. Benton, O. Sikora, and N. Shannon. Seeing the light: Experimental signatures of emergent electromagnetism in a quantum spin ice. *Phys. Rev. B*, 86:075154, Aug 2012.

[24] M.J.P. Gingras and P.A. McClarty. Quantum spin ice: a search for gapless quantum spin liquids in pyrochlore magnets. *Reports on Progress in Physics*, 77(5):056501, May 2014.

[25] F. Mila. Quantum spin liquids. *European Journal of Physics*, 21(6):499, Nov 2000.

[26] P.W. Anderson. Resonating valence bonds: A new kind of insulator? *Materials Research Bulletin*, 8(2):153–160, Feb 1973.

[27] P. W. Anderson, G. Baskaran, Z. Zou, and T. Hsu. Resonating – valence-bond theory of phase transitions and superconductivity in La_2CuO_4-based compounds. *Phys. Rev. Lett.*, 58:2790–2793, Jun 1987.

[28] H. Nishimori and G. Ortiz. *Elements of Phase Transitions and Critical Phenomena*. Oxford University Press, 2010.

[29] J. G. Bednorz and K. A. Müller. Possible high superconductivity in the balacuo system. *Zeitschrift für Physik B Condensed Matter*, 64:189–193, 1986. 10.1007/BF01303701.

[30] P.W. Anderson. Is there glue in cuprate superconductors? *Science (New York, NY)*, 316(5832):1705, Jun 2007.

[31] P.W. Anderson. The resonating valence bond state in La_2CuO_4 and superconductivity. *Science*, 235(4793):1196–1198, Mar 1987.

[32] Xiao-Gang Wen. *Quantum Field Theory of Many-body Systems from the Origin of Sound to an Origin of Light and Electrons*, volume 1. Oxford University Press Inc., 2004.

[33] Y.-P. Huang, G. Chen, and M. Hermele. Quantum spin ices and topological phases from dipolar-octupolar doublets on the pyrochlore lattice. *Phys. Rev. Lett.*, 112:167203, Apr 2014.

[34] A.Y. Kitaev. Fault-tolerant quantum computation by anyons. *Annals of Physics*, 303(1):2–30, Jan 2003.

[35] C. Nayak, S. H. Simon, A. Stern, M. Freedman, and S. Das Sarma. Non-abelian anyons and topological quantum computation. *Rev. Mod. Phys.*, 80:1083–1159, Sep 2008.

[36] B. Javanparast, A.G.R Day, Z. Hao, and M.J.P. Gingras. Thermal order-by-disorder at criticality in xy pyrochlore magnets. *unpublished*.

[37] D. C. Tsui, H. L. Stormer, and A. C. Gossard. Two-dimensional magnetotransport in the extreme quantum limit. *Phys. Rev. Lett.*, 48:1559–1562, May 1982.

[38] X.-G. Wen. Quantum orders and symmetric spin liquids. *Phys. Rev. B*, 65:165113, Apr 2002.

[39] B.A. Bernevig. *Topological Insulators and Topological Superconductors*. Princeton University Press, 2013.

[40] S. Yan, D.A. Huse, and S.R. White. Spin-liquid ground state of the $s = 1/2$ kagome heisenberg antiferromagnet. *Science*, 332(6034):1173–1176, Jun 2011.

[41] G. Baskaran, Z. Zou, and P.W. Anderson. The resonating valence bond state and high-tc superconductivity — a mean field theory. *Solid State Communications*, 63(11):973 – 976, 1987.

[42] X.-G. Wen. Origin of gauge bosons from strong quantum correlations. *Phys. Rev. Lett.*, 88:011602, Dec 2001.

[43] I. Affleck and J.B. Marston. Large-n limit of the heisenberg-hubbard model: Implications for high-t_c superconductors. *Physical Review B*, 37(7):3774, Mar 1988.

[44] F. J. Burnell, S. Chakravarty, and S. L. Sondhi. Monopole flux state on the pyrochlore lattice. *Phys. Rev. B*, 79:144432, Apr 2009.

[45] U. Schollwöck. The density-matrix renormalization group. *Rev. Mod. Phys.*, 77:259–315, Apr 2005.

[46] A. W. Sandvik. Computational studies of quantum spin systems. 1297:135–338, November 2010.

[47] P. Henelius and A.W Sandvik. Sign problem in monte carlo simulations of frustrated quantum spin systems. *Physical Review B*, 62(2):1102, Jul 2000.

[48] C. Gros. Physics of projected wavefunctions. *Annals of Physics*, 189(1):53–88, Jan 1989.

[49] Daniel S. Rokhsar and Steven A. Kivelson. Superconductivity and the quantum hard-core dimer gas. *Phys. Rev. Lett.*, 61:2376–2379, Nov 1988.

[50] D.A. Huse, W. Krauth, R. Moessner, and S. L. Sondhi. Coulomb and liquid dimer models in three dimensions. *Phys. Rev. Lett.*, 91:167004, Oct 2003.

[51] E. Fradkin and S. Kivelson. Short range resonating valence bond theories and superconductivity. *Modern Physics Letters B*, 4(03):225–232, Feb 1990.

[52] E. Fradkin, D.A. Huse, R. Moessner, V. Oganesyan, and S.L. Sondhi. Bipartite rokhsar–kivelson points and cantor deconfinement. *Phys. Rev. B*, 69(22):224415, Jun 2004.

[53] A. Banerjee, S. V. Isakov, K. Damle, and Y. B. Kim. Unusual liquid state of hard-core bosons on the pyrochlore lattice. *Phys. Rev. Lett.*, 100:047208, Jan 2008.

[54] N. Shannon, O. Sikora, F. Pollmann, K. Penc, and P. Fulde. Quantum ice: A quantum monte carlo study. *Phys. Rev. Lett.*, 108:067204, Feb 2012.

[55] J. S. Gardner, M. J. P. Gingras, and J. E. Greedan. Magnetic pyrochlore oxides. *Rev. Mod. Phys.*, 82:53–107, Jan 2010.

[56] S.H. Curnoe. Structural distortion and the spin liquid state in $Tb_2Ti_2O_7$. *Physical Review B*, 78(9):094418, Sep 2008.

[57] K. A. Ross, L. Savary, B. D. Gaulin, and L. Balents. Quantum excitations in quantum spin ice. *Phys. Rev. X*, 1:021002, Oct 2011.

[58] J.A. Hodges, P. Bonville, M. Forget, A. Rams, Królas K., and G. Dhalenne. The crystal field and exchange interactions in $Yb_2Ti_2O_7$. *J. Phys.: Condens. Matter*, 13(41), Sep 2001.

[59] J. D. M. Champion, M. J. Harris, P. C. W. Holdsworth, A. S. Wills, G. Balakrishnan, S. T. Bramwell, E. Cizmar, T. Fennell, J. S. Gardner, J. Lago, D. F. McMorrow, M. Orendac, A. Orendacova, D. M. Paul, R. I. Smith, M. T. F. Telling, and A. Wildes. $Er_2Ti_2O_7$ evidence of quantum order by disorder in a frustrated antiferromagnet. *Phys. Rev. B*, 68:020401, Jul 2003.

[60] L. Savary, K. A. Ross, B. D. Gaulin, J. P. C. Ruff, and L. Balents. Order by quantum disorder in $Er_2Ti_2O_7$. *Physical review letters*, 109(16):167201, Oct 2012.

[61] P. Stasiak, P. A. McClarty, and M. J. P. Gingras. Order-by-Disorder in the XY Pyrochlore Antiferromagnet Revisited. *ArXiv e-prints*, August 2011.

[62] M. E. Zhitomirsky, M. V. Gvozdikova, P. C. W. Holdsworth, and R. Moessner. Quantum order by disorder and accidental soft mode in $er_2ti_2o_7$. *Phys. Rev. Lett.*, 109:077204, Aug 2012.

[63] J. Oitmaa, R. R. P. Singh, B. Javanparast, A. G. R. Day, B. V. Bagheri, and M. J. P. Gingras. Phase transition and thermal order-by-disorder in the pyrochlore antiferromagnet $Er_2Ti_2O_7$: A high-temperature series expansion study. *Phys. Rev. B*, 88:220404, Dec 2013.

[64] R. Applegate, N. R. Hayre, R. R. P. Singh, T. Lin, A. G. R. Day, and M. J. P. Gingras. Vindication of $yb_2ti_2o_7$ as a model exchange quantum spin ice. *Phys. Rev. Lett.*, 109:097205, Aug 2012.

[65] H. R. Molavian, M. J. P. Gingras, and B. Canals. Dynamically induced frustration as a route to a quantum spin ice state in $Tb_2Ti_2O_7$ via virtual crystal field excitations and quantum many-body effects. *Physical review letters*, 98(15):157204, Apr 2007.

[66] H.R. Molavian and M.J.P. Gingras. Proposal for a [111] magnetization plateau in the spin liquid state of tb2ti2o7. *J. Phys.: Condens. Matter*, 21(17), Apr 2009.

[67] H.R. Molavian, P.A. McClarty, and M.J.P. Gingras. Towards an effective spin hamiltonian of the pyrochlore spin liquid $Tb_2Ti_2O_7$. *ArXiv e-prints*, 2009.

[68] S.P. Mukherjee and S.H. Curnoe. Effective spin-1/2 exchange interactions in $Tb_2Ti_2O_7$. *ArXiv e-prints*, 2014.

[69] L. Savary and L. Balents. Spin liquid regimes at nonzero temperature in quantum spin ice. *Phys. Rev. B*, 87:205130, May 2013.

[70] L.-P. Henry and T. Roscilde. Order-by-disorder and quantum Coulomb phase in quantum square ice. *ArXiv e-prints*, July 2013.

[71] K.G. Wilson. Confinement of quarks. *Phys. Rev. D*, 10:2445–2459, Oct 1974.

[72] S. Elitzur. Impossibility of spontaneously breaking local symmetries. *Physical Review D*, 12(12):3978, Dec 1975.

[73] E. Fradkin and S.H. Shenker. Phase diagrams of lattice gauge theories with higgs fields. *Phys. Rev. D*, 19:3682–3697, Jun 1979.

[74] A.M. Polyakov. *Gauge Fields and Strings (Contemporary Concepts in Physics)*. Harwood Academic Publishers, Switzerland, 1987.

[75] A. Auerbach. *Interacting electrons and quantum magnetism*. Springer, 1994.

[76] S. Sachdev. *Quantum Phase Transitions*. Cambridge University Press, 2001.

[77] J.-W. Mei, E. Tang, and X.-G. Wen. Chiral spin states in polarized kagome spin systems with spin-orbit coupling. *ArXiv e-prints*, February 2011.

[78] Y.-F. Wang, Z.-C. Gu, C.-D. Gong, and D. N. Sheng. Fractional quantum hall effect of hard-core bosons in topological flat bands. *Phys. Rev. Lett.*, 107:146803, Sep 2011.

[79] A. S. Nowick. *Crystal properties via group theory*. Cambridge University Press, 2005.

[80] I. Lindgren and J. Morrison. *Atomic many-body theory*. Springer, 1986.

[81] A. L. Chernyshev, D. Galanakis, P. Phillips, A. V. Rozhkov, and A.-M. S. Tremblay. Higher order corrections to effective low-energy theories for strongly correlated electron systems. *Phys. Rev. B*, 70:235111, Dec 2004.

[82] N. W. Ashcroft and N. D. Mermin. *Solid State Physics*. Brooks/Cole, 1976.